Article

The International Journal of Robotics Research
32(13) 1585–1606

DOI: 10.1177/0278364913498122
ijr.sagepub.com

Foot–terrain interaction mechanics for legged robots: Modeling and experimental validation

Liang Ding[1], Haibo Gao[1], Zongquan Deng[1], Jianhu Song[2], Yiqun Liu[1], Guangjun Liu[3], and Karl Iagnemma[4]

Abstract

Contact mechanics plays an important role in the design, performance analysis, simulation, and control of legged robots. The Hunt–Crossley model and the Coulomb friction model are often used as black-box models with limited consideration of the properties of the terrain and the feet. This paper analyzes the foot–terrain interaction based on the knowledge of terramechanics and reveals the relationship between the parameters of the conventional models and the terramechanics models. The proposed models are derived in three categories: deformable foot on hard terrain, hard foot on deformable terrain, and deformable foot on deformable terrain. A novel model of tangential forces as the function of displacement is proposed on the basis of an in-depth understanding of the terrain properties. Methods for identifying the model parameters are also developed. Extensive foot–soil interaction experiments have been carried out, and the experimental results validate the high fidelity of the derived models.

Keywords

Legged robots, terramechanics, contact mechanics model, parameter identification

1. Introduction

Legged robots are playing increasingly important roles in the field activities of humankind after many years of development (Hardarson, 1997). Exciting examples that have come forth recently include the two-legged PETMAN for disaster response (Ackerman, 2012), the four-legged COMET-IV for mine detection (Irawan and Nonami, 2011), BigDog (Raibert et al., 2008), LS3 (BostonDynamics, 2012a), and TITAN XI (Shigeo et al., 2009) for field applications, the six-legged ATHLETE for planetary exploration (Wilcox et al., 2007), and the Plustech walking robot for harvesting trees in forests (Maclou, 2012).

Many of the current and future legged robots are expected to traverse challenging field terrains that are neither structured nor flat and hard. Contact mechanics (Gilardi and Sharf, 2002) plays a fundamental role in the development of legged robots. Wheeler et al. (2010) used a three-dimensional Hunt–Crossley model (Hunt and Crossley, 1975) to predict the mechanics of the ATHLETE robots. Interaction forces and the corresponding deformation are calculated with the wheels modeled as three-dimensional springs. Silva et al. (2009) presented a genetic algorithm running over a simulation application for legged robots, which optimizes several parameters of the robot and its gait. The contact of the robot's feet with the ground is modeled with linear stiffness and nonlinear damping in both the horizontal and vertical directions, and the model parameters for several types of terrains are summarized (Silva et al., 2005). Fujimoto and Kawamura (1998) realized the dynamic simulation for a biped walking robot, considering the interaction force with the environment. Irawan and Nonami (2011) presented the implementation of impedance control on COMET-IV, a hydraulically driven hexapod robot, in order to make it walk on uneven and extremely soft terrain, and the terrain was considered as spring and damping to generate interaction forces that act on the feet. Palis

[1]State Key Laboratory of Robotics and System, Harbin Institute of Technology, Harbin, Heilongjiang, the People's Republic of China.
[2]Antenna and Servo Department, the 54th Research Institute of China Electronics Technology Group Corporation, Shijiazhuang, Hebei, the People's Republic of China.
[3]Department of Aerospace Engineering, Ryerson University, Toronto, ON, Canada.
[4]Laboratory for Manufacturing and Productivity, Massachusetts Institute of Technology, Cambridge, MA, USA

Corresponding author:
Haibo Gao, State Key Laboratory of Robotics and System, Harbin Institute of Technology, Harbin 150001, Heilongjiang, the People's Republic of China.
Email: gaohaibo@hit.edu.cn, liangding@hit.edu.cn

et al. (2005) also proposed an impedance control algorithm to increase the adaptability of a multi-legged robot on irregular terrain and to distribute the foot forces.

The Hunt–Crossley model is a general nonlinear contact model incorporating both penetration and velocity, and many other contact models can be considered its special cases (Ding et al., 2013b). The Hunt–Crossley model is used by some researchers to predict the three-dimensional interaction force, but the forces in the tangential direction are different in essence from the force in the normal direction. An obvious distinction is that the tangential force is usually considered as the function of the normal force, but the normal force is little influenced by the tangential force. Instead, the Coulomb friction model (Trinkle et al., 1997) and its improved versions are usually adopted to predict the tangential interaction force. Mahapatra and Roy (2009) used the contact model of ADAMS, which includes the Coulomb friction model in the tangential direction and the Hunt–Crossley model in the normal direction, to simulate the motion of a six-legged robot. Hurmuzlu et al. (2004) used the Amontons–Coulomb law to predict the tangential force in order for the modeling, stability analysis, and control of the biped robots.

The general models for predicting the contact force in the normal direction and tangential direction are not particular to robots' feet, and they are used to study the interaction mechanics of other robotic systems (Misra et al., 2010; Shapiro et al., 2004; Sharf et al., 2009) and mechanical systems (Song et al., 2000; Lankarani and Nikravesh, 1990). The applicability of such models to various situations is ensured by parameter identification (Sharf et al., 2009; Biagiotti et al., 2005; Diolaiti et al., 2005), and the parameters might not map directly to the physically measurable quantities, including the properties of the robot (such as shape, width, length) and the environment (such as soil parameters), but rather to combinations of physical parameters.

Terramechanics deals with the interaction mechanics of conventional terrestrial vehicles and their terrain, and it has been widely applied to the interaction mechanics of wheeled mobile robots (Ding et al., 2011a). The works of Bekker (1969), Wong and Reece (1967), Janosi and Hanamoto (1961), among others, provide fundamental terramechanics models. Using the knowledge of terramechanics, not only the interaction mechanics of the feet on the deformable terrain could be predicted (a preliminary example is provided by Komizunai et al., 2011) but also the parameters of the models could be revealed using the property parameters of the terrain and the feet.

This paper aims at the development of models and parameter identification methods for foot–terrain interaction on the basis of terramechanics. The main contributions of this paper include the following: (1) interaction mechanics models of robots' feet with deformable terrains, using parameters directly related to the feet and soil properties; (2) a novel model of tangential forces based on the stress distribution of deformable soil, which is the function of displacement, different from the conventional models; (3) approaches of identifying interaction mechanics parameters for foot (hard and deformable) and terrain (hard and deformable) with different properties; and (4) comprehensive experimental studies of foot–terrain interaction and model validation.

The rest of the paper is organized as follows. Section 2 summarizes the preliminary knowledge of foot–terrain interaction mechanics. Section 3 presents the interaction mechanics models, including a deformable (hard) foot versus hard (deformable) terrain and a deformable foot versus deformable terrain. The parameter identification methods for such models are further provided in Section 4. Finally, validation experiments are presented in Section 5, and conclusions are given in Section 6.

2. Analysis of foot–terrain interaction

The generalized foot–terrain interaction model and the properties of feet and the terrain that influence the interaction mechanics are addressed in this section.

2.1. Generalized foot–terrain interaction model

Upon the interaction of a foot with a deformable terrain, three forces and three moments are generated on the foot, as shown in Figure 1. The coordinate of the interaction mechanics is denoted by O-xyz, the origin O of which is at the plane of terrain surface (tangential plane), the z axis of which is perpendicular to the terrain surface, and the x axis of which is aligned with the direction of the robot's body. The normal force, F_{N}, caused by the deformation of the foot and/or the terrain, can sustain the foot. The tangential force has a direction opposite to the velocity of the foot on the terrain and can be decomposed into the tractive force F_x and the lateral force F_y. The included angle between the direction of the foot and that of the velocity on the terrain is called the slip angle, denoted by β. There are also three moments that act on the foot due to interaction with the terrain, which are denoted by M_x, M_y, and M_z. If the distance between the origin of the coordinate O-xyz and the terrain is small, the moments can be neglected for simplification, otherwise the moments can be approximated by the products of the forces and their related arms.

The foot–terrain interaction forces and moments are influenced by the physical and mechanical properties of the terrain or the soil, the parameters of which are denoted by P_{T}, the foot property parameters P_{F}, the terrain geometry parameters P_{G}, and the motion state variables P_{M} (such as the displacement and the velocity). The generalized form of

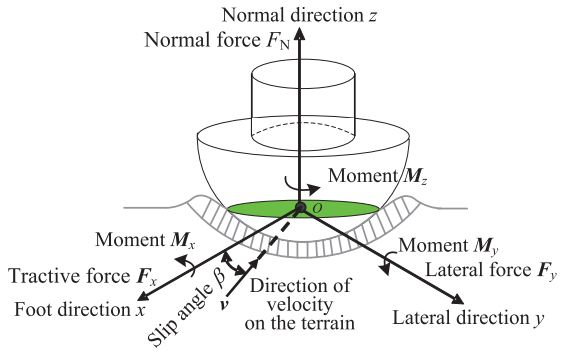

Fig. 1. Generalized foot–terrain interaction mechanics model.

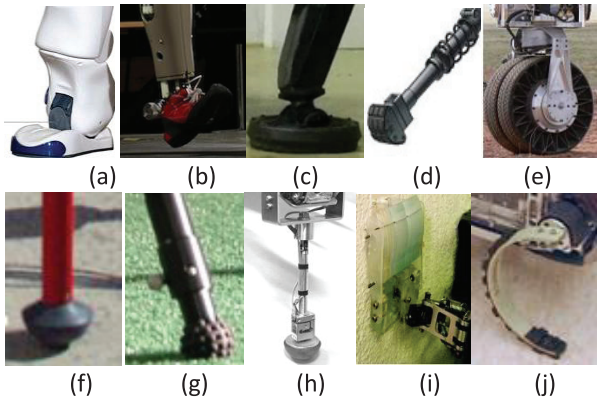

Fig. 2. Typical robots' feet.

foot–terrain interaction mechanics can be expressed as

$$\begin{cases} F_N = F_N(P_T, P_F, P_G, P_M) \\ F_x = F_x(P_T, P_F, P_G, P_M) \\ F_y = F_y(P_T, P_F, P_G, P_M) \\ M_x = M_x(P_T, P_F, P_G, P_M) \\ M_y = M_y(P_T, P_F, P_G, P_M) \\ M_z = M_z(P_T, P_F, P_G, P_M) \end{cases} \quad (1)$$

2.2. Characteristics of the robots' feet

The characteristics of a robot foot, denoted by P_F, including the shape, dimension, and material, obviously have an influence on the interaction mechanics. Figure 2 shows some typical robots' feet.

The shapes of typical robot feet are summarized in Table 1. Many robots' feet are flat in order to obtain a large contact area with the flat terrain. The feet of most humanoid robots are flat with a rectangular (or approximately) shape, such as ASIMO, NAO, Elvina, and PETMAN. If a legged robot is expected to move on rough terrain, the feet are usually designed with a cylindrical or spherical shape so that they can adapt to the terrain more freely, with examples including the BigDog, LS3, SILO6, LittleDog, and SLAIR. The feet of ATHLETE are actually stationary wheels when it walks so that they are also cylindrical. The feet of some robots are irregular in shape, especially when they have a bio-inspired structure, such as the robots of RHex, RiSE and eQuad.

Table 1. Typical shapes of robots' feet and examples.

Shape of foot	Examples
Flat	ASIMO (Watanabe et al., 2002); NAO, Figure 1(a) (Sanchez, 2009); Elvina (Wahde and Pettersson, 2002); PETMAN, Figure 1(b) (Ackerman, 2012); TITAN (Shigeo et al., 2009); Plustech walking robot, Figure 1(c) (Maclou, 2012), COMET-IV (Irawan and Nonami, 2011) BigDog, Fig. 1 (d) (Raibert et al. 2008);
Cylindrical	BigDog, Figure 1(d) (Raibert et al., 2008); LS3 (BostonDynamics, 2012a); ATHLETE, Figure 1(e) (Wilcox et al., 2007)
Spherical	SILO6, Figure 1(f) (Santos et al., 2007); LittleDog, Figure 1(g) (BostonDynamics, 2012b); SLAIR, Figure 1(h) (Palis et al., 2005)
Irregular	RHex, Figure 1(i) (Spagna et al., 2007); RiSE, Figure 1(j) (Spenko et al., 2008); eQuad (Sun and Ma, 2011)

The foot sizes of the robots are also quite different from one another. The parameters for the rectangular flat feet are characterized by width b and length l. The foot dimensions of PETMAN are similar to those of an adult; the dimensions of the feet of Asimo and NAO are smaller. The foot dimensions of robots with larger payload specification are also larger. The feet of some robots are rather small, including LittleDog, BigDog, and SLAIR. The dimensions of robots' feet are typically determined by the maximum load that acts on the feet from the interaction with the terrain, which is related to the weight and payload of the robot as well as the number of feet. Table 2 shows the parameters of some legged robots.

In order to decrease the impact while the feet make contact with the terrain, spring and damping components are usually embedded in the feet or the legs, which obviously influence the interaction mechanics. For example, there are springs installed in the legs of BigDog, and the feet of SILO6 and LittleDog have cushion materials at the bottom.

2.3. Terrain characteristics

The terrain characteristics include the mechanical properties represented by P_T, as well as the terrain geometry parameters represented by P_G. A flat and hard terrain is assumed in the early works on legged robots. However, legged robots are superior to wheeled and tracked robots because they can traverse rough terrain. Many recently developed legged robots are expected to work in fields with rough terrain. The geometry of terrain is divided into flat and rough, whereas the physical properties of terrain can be categorized as hard and deformable. Hard terrain includes stairs, gravels, ruins, and structured hard surfaces; typical deformable terrain includes the forest, planetary surface,

Table 2. Parameters of typical legged robots (Raibert et al., 2008; Wilcox et al., 2007, Santos et al., 2007; Carbone and Ceccarelli, 2005).

Name of robot	Number of feet	Size of robot (m × m × m)	Weight (N)	Maximum speed (m/s)	Payload (N)
ASIMO (Carbone and Ceccarelli, 2005)	2	1.2 × 0.4 × 0.5	520	0.4	5
SDR-4X (Carbone and Ceccarelli, 2005)	2	0.6 × 0.3 × 0.2	70	0.3	0
WABIAN-RV (Carbone and Ceccarelli, 2005)	2	1.8 × 0.4 × 0.6	1,300	0.3	10
WL-16 (Carbone and Ceccarelli, 2005)	2	1.3 × 0.3 × 0.6	620	0.3	600
RIMHO2 (Carbone and Ceccarelli, 2005)	4	0.7 × 0.7 × 0.3	650	0.1	0
Scout II (Carbone and Ceccarelli, 2005)	4	0.4 × 0.4 × 0.4	270	1.5	5
WorkPartner (Carbone and Ceccarelli, 2005)	4	1.4 × 1.2 × 1.2	2,300	1.94	100
RHex (Carbone and Ceccarelli, 2005)	6	0.5 × 0.2 × 0.1	70	0.4	0
A.S.V. (Carbone and Ceccarelli, 2005)	6	5.2 × 2.4 × 3.0	32,000	2.0	2,156
W.F.M. (Carbone and Ceccarelli, 2005)	6	7.4 × 2.7 × 3.7	34,000	2.0	2,000
AIBO (Carbone and Ceccarelli, 2005)	4	0.2 × 0.3 × 0.3	16.5	0.3	0
BigDog (Raibert et al., 2008)	4	1.0 × 1.1 × 0.3	1,090	2.0	1,540
SILO6 (Santos et al., 2007)	6	0.88 × 0.45 × 0.2	699	1.4	0
ATHLETE (Quarter-scale SDM)(Wilcox et al., 2007)	6	2.75 × 2.75 × 2.08	8,330 (SDM)	2.78	Several thousand

lawn, snow, and sand. Examples of terrain and the related robots are listed in Table 3 and illustrated in Figure 3.

3. Models of foot–terrain interaction

The contact mechanics models of foot–terrain interaction are usually divided into normal force models and tangential force models. In the normal direction, the interaction force is usually approximated by the force on the spring and the damper of the foot; in the tangential direction, the force is usually calculated with the Coulomb frictional model or its improved versions. The three-dimensional spring–damping models are also used sometimes.

Actually, in the tangential plane, the force direction is opposite to the motion direction of the foot, which could be decomposed into two forces in the local coordinates of the foot. Figure 4 shows that a wheeled-type foot acts on a deformable terrain, where α_1 and α_2 are the slope angles, φ_F is the inclined angle of x_1 (the x axis of the inertia coordinate) to the horizontal projection of the foot's direction (the x axis of the foot coordinate), β_F is the inclined angle between the foot direction and the force direction (i.e. the opposite direction of the foot's velocity $\boldsymbol{v}$), and F_T denotes the force in the tangential plane.

Suppose that the normal vector of the contact surface is $P_G = \{A_t, B_t, C_t\}$. The equivalent force on the foot as described in the inertial coordinate is as follows:

$$^{I}\boldsymbol{F} = {}^{I}\boldsymbol{A}_{F}{}^{F}\boldsymbol{F}. \tag{2}$$

In Equation (2), ${}^{I}\boldsymbol{A}_F$ is the transition matrix from the foot coordinate to the inertia coordinate (Ding et al., 2010):

$$^{I}\boldsymbol{A}_F = \begin{bmatrix} \frac{C_t}{X_1} & \frac{-A_tB_t-(B_t^2+C_t^2)\tan\varphi_w}{X_2} & \frac{A_t}{X_3} \\ \frac{C_t\tan\varphi_w}{X_1} & \frac{C_t^2+A_t^2+A_tB_t\tan\varphi_w}{X_2} & \frac{B_t}{X_3} \\ \frac{-A_t-B_t\tan\varphi_w}{X_1} & \frac{A_tC_t\tan\varphi_w-B_tC_t}{X_2} & \frac{C_t}{X_3} \end{bmatrix}. \tag{3}$$

Table 3. Typical terrains for legged robots.

Characteristics of terrain	Examples
Hard	Stairs, Figure 3 (a) (Wahde and Pettersson, 2002); gravels; ruin, Figure 3 (b) (Raibert et al., 2008); structured terrain, Figure 3 (c) (Shigeo et al., 2009), etc.
Deformable	Forest, Figure 3 (d) (Maclou, 2012); planetary surface, Figure 3 (e) (Wilcox e al., 2007); lawn; snow, Figure 3 (f) (Raibert et al., 2008); sand (Komizunai et al., 2011), etc.

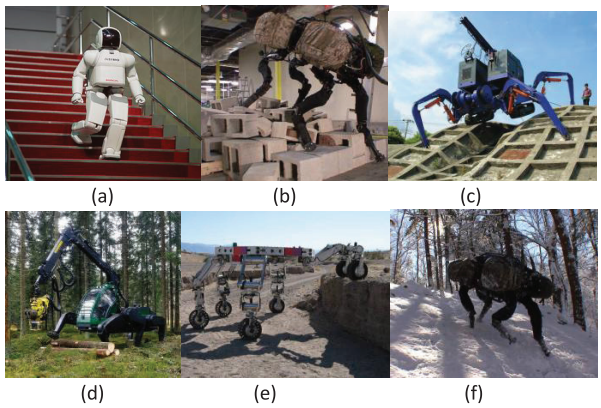

Fig. 3. Typical terrain for legged robots: (a) stairs (Wahde and Pettersson, 2002); (b) ruins (Raibert et al., 2008); (c) structured terrain (Shigeo et al., 2009); (d) forest (Maclou, 2012); (e) sand (Wilcox et al., 2007); (f) snow (Raibert et al., 2008).

where

$$\begin{cases} X_1 = \sqrt{C_t^2(1+\tan^2\varphi_w)+(A_t+B_t\tan\varphi_w)^2} \\ X_2 = \sqrt{X_3^2[A_t^2+C_t^2+2A_tB_t\tan\varphi_t+(B_t^2+C_t^2)\tan^2\varphi_w]} \\ X_3 = \sqrt{A_t^2+B_t^2+C_t^2} \end{cases}$$

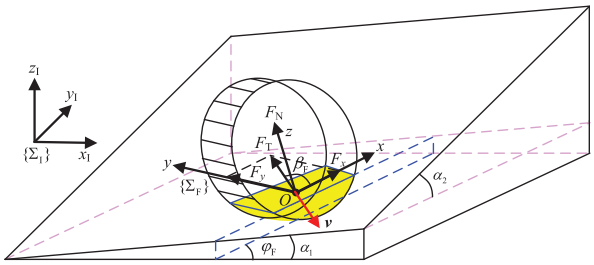

Fig. 4. Coordinate system for foot–terrain interaction mechanics on the slope (Ding et al., 2010).

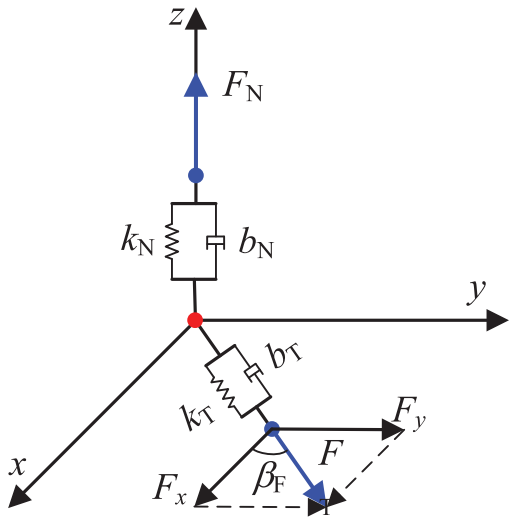

Fig. 5. A three-dimensional interaction mechanics model.

A conventional three-dimensional model divides the deformation of the foot or the terrain into two orthogonal directions in the tangential plane, which neglects the coupling effect of the deformation and, thus, leads to obvious errors. In order to take into account the coupling effect, a novel three-dimensional foot–terrain interaction mechanics model is proposed:

$$\begin{cases} F_z = F_N \\ F_x = F_T \cos\beta_F \\ F_y = F_T \sin\beta_F \end{cases}. \tag{4}$$

Figure 5 illustrates the concept of the proposed model in the tangential plane.

The remaining problem is to calculate the normal force F_N and the tangential force F_T that the terrain exerts on the foot. In Figure 5, the tangential force and the normal force, which are modeled using nonlinear springs and dampers, are only taken as examples. The actual equations of predicting the forces depend on the properties of the foot and the terrain, which is to be investigated further in this paper.

Figure 6 shows the interaction of a robot's foot with the terrain in the normal direction using the spring–damping model, where F_{FN} is the effective normal force that acts on the body of a robot by the foot, F_{TN} is the normal force that

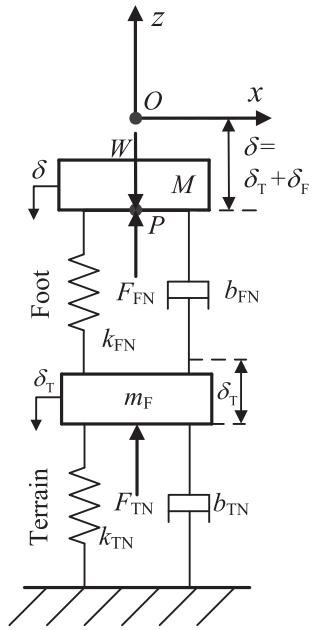

Fig. 6. Interaction of a robot's foot with the terrain in the normal direction.

acts on the foot by the terrain, m_F is the mass of the foot, W is the normal load exerted on the foot, δ_T and δ_F are the deformation of the terrain and the foot, respectively, and δ is their summation. Hence,

$$F_N = F_{FN} = F_{TN} - m_F g + m_F \ddot{\delta}_T. \tag{5}$$

If the spring is linear without damping, the static equilibrium equation of Figure 6 is expressed as follows:

$$F_N = k_{FN}\delta_F = k_{TN}\delta_T, \tag{6}$$

where k_{FN} is the normal rigidity coefficient of the foot and k_{TN} is the normal rigidity coefficient of the terrain. Then, $\delta = \delta_F + \delta_T = F_N/k_{FN} + F_N/k_{TN}$. The equivalent equation of the contact mechanics between the foot and the terrain is as follows: $F_N = \delta/(1/k_{FN} + 1/k_{TN})$. Then, the equivalent spring coefficient is as follows:

$$k_N = (k_{FN} + k_{TN})/(k_{FN}k_{TN}). \tag{7}$$

Table 4 shows the rigidity coefficients and damping coefficients of some typical terrain (Silva et al., 2005). It can be seen that the rigidity coefficients of different terrains are quite different, which decrease from the term of $10^9 \mathrm{Nm}^{-1}$ (concrete and wood) to $10^5 \mathrm{Nm}^{-1}$ (loose clay). If $k_{FN} >> k_{TN}$, i.e. the foot is much harder than the terrain, then the contact force is primarily determined by the deformation of the terrain, otherwise, if $k_{FN} << k_{TN}$, the contact force is primarily determined by the deformation of the foot. Considering the properties of both the foot and the terrain, the interaction between them can be divided into four categories: (1) a hard foot versus hard terrain, (2) a deformable foot versus hard terrain, (3) a hard foot versus deformable terrain, and (4) a deformable foot versus deformable terrain.

Table 4. Typical terrain parameters (Silva et al., 1998).

Terrain type	Young's modulus ($kN\,m^{-2}$)	k_{TN}($N\,m^{-1}$)	b_{TN}($Ns\,m^{-1}$)	k_{TT}($N\,m^{-1}$)	b_{TT}($Ns\,m^{-1}$)
Concrete	3×10^7	3.4×10^9	1.8×10^5	2.6×10^9	1.5×10^5
Wood	1.3×10^7	1.5×10^9	1.2×10^5	1.1×10^9	1.0×10^5
Gravel	$(1–2) \times 10^5$	2.3×10^7	1.4×10^4	1.7×107	1.2×10^4
Sand	$(1–8) \times 10^4$	9.1×10^6	9.0×10^3	6.9×10^6	7.9×10^3
Compact clay	$(3–15) \times 10^3$	1.7×10^6	3.9×10^3	1.3×10^6	3.4×10^3
Loose clay	$(5–30) \times 10^2$	3.4×10^5	1.8×10^3	2.6×10^5	1.5×10^3

The interaction between a hard foot and a hard terrain could be destructive, and proper mechanisms may have to be used for protecting the foot. But one cannot avoid such scenarios in natural environments if a hard foot is used. According to Gilardi and Sharf (2002), the interaction between two rigid bodies is known as an "impact" in the literature, which is a complex physical phenomenon occurring when two or more bodies collide with each other; characteristics of impact are very brief duration, high force levels, rapid dissipation of energy, and large accelerations and decelerations. Newton's model, Poisson's model, and Strong's model are usually employed (Gilardi and Sharf, 2002; Stronge, 1991; Stewart, 2000) to predict the process of energy transfer and dissipation, using various coefficients including the coefficient of restitution and the impulse ratio. The collision process is much more complex when the friction exists. The two-dimensional nonlinear interaction effect between the static friction coefficient and the coefficient of restitution in rigid body collisions, as well as the complexities arising from slip and slip reversal, are considered by Stronge (1990), Wang and Mason (1992), Stewart (2000), and Nanayakkara et al. (2012).

The compliant contact mechanics falls under a class of interaction mechanics different from the impact mechanics between rigid bodies. The term "contact", which implies a continuous process that takes place over a finite time (Gilardi and Sharf, 2002), is usually used. This paper focuses on the other three compliant interaction processes, as described above in situations (2), (3) and (4). The compliant models could be further developed to explain rigid-body collisions with special assumptions. Kraus and Kumar (1997) provided a good example based on the traditional Hunt–Crossley model.

3.1. Deformable foot versus hard terrain

If the foot is deformable and the terrain is hard with little deformation, the normal force can be considered as the function of the foot's deformation and its velocity. The typical nonlinear spring–damping model developed by Hunt and Crossley can be used (Hunt and Crossley, 1975):

$$F = k\delta^n + b\delta^p\dot{\delta}^q. \tag{8}$$

Table 5. Normal force models and parameters (Ding et al., submitted).

Model name	Unknown parameters	Known parameters
Hunt-Crossley model	k, b, n, p, q	–
Simplified Hunt-Crossley model	k, b, n	$p = n, q = 1$
Linear spring–damping model	k, b	$n = 1, q = 1, p = 0$
Hertz's model	k, n	$b = 0$
Spring model	k	$n = 1, b = 0$

The Hunt–Crossley model includes five parameters: k, the rigidity coefficient; b, the damping coefficient; n, the exponent of the rigidity term; and p and q, the exponents of the damping term, which could be identified on the basis of the experimental results for the prediction of the normal force according to δ and its velocity. A standard simplification is $p = n$ and $q = 1$; then, there are only three unknown parameters. The five unknown parameters can be further simplified to obtain a linear spring-damping model, Hertz's model, and the spring model, as shown in Table 5. The more the unknown parameters, the more are the experimental data required for identifying them and the higher is the precision of the corresponding models.

The normal force generated by the deformable foot is as follows:

$$F_N = F_{FN} = k_{FN}\delta^{n_{FN}} + b_{FN}\delta^{p_{FN}}\dot{\delta}^{q_{FN}}, \tag{9}$$

where the subscript FN denotes the foot in the normal direction.

In the tangential plane, if a slip occurs, the tangential force is actually the friction force between the foot and the terrain. The Coulomb friction model can be used to predict the tangential force F_T (Olsson et al., 1998):

$$F_T = \begin{cases} F_e & (v = 0 \text{ and } |F_e| \le \mu_s F_{TN}) \\ \mu F_{TN}\mathrm{sgn}(v) & (v \ne 0) \\ \mu_s F_{TN}\mathrm{sgn}(F_e) & (\text{Otherwise}) \end{cases}. \tag{10}$$

where F_e is the equivalent external force in the tangential plane that is exerted on a foot by the leg. If the foot is static during the contact with the terrain, the force F_T equals to F_e (when $F_e \le \mu_s F_{TN}$) or $\mu_s F_{TN}$ sgn(F_e). If the foot is moving

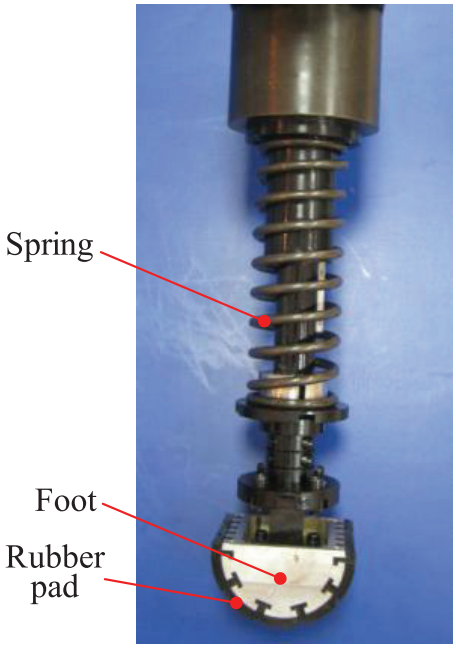

Fig. 7. Foot of a four-legged robot.

on the terrain, the force is equals to $\mu_s F_{TN} \mathrm{sgn}(v)$. In Equation (10), the static frictional coefficient μ_s is larger than the frictional coefficient μ and there is an abrupt change when the foot begins to move from the static state. What makes it more difficult is that the coefficient μ_s is hard to determine.

If the velocity is zero but there is an external force, the force F_T is equal to the external force. From the microcosmic viewpoint, this force is actually generated by the deformation at the contact surface, so this could also be calculated using the Hunt–Crossley model if the deformation of the foot in the tangential direction is obvious as compared with the slip between the foot and the terrain. However, the Hunt–Crossley model does not contain the normal force. Therefore, the Hunt–Crossley model and the Coulomb model are combined to predict the tangential force:

$$F_T = \begin{cases} k_{FT} j^{n_{FT}} + b_{FT} j^{p_{FT}} \dot{j}^{q_{FT}} & (F_T \le \mu F_N) \\ \mu F_{TN} \mathrm{sgn}(v) & (\text{Otherwise}) \end{cases}, \tag{11}$$

where j is the horizontal deformation of the foot and the friction coefficient μ is determined by the friction property of the foot's surface and the terrain. The Hunt–Crossley model parameters in Equation (11) are determined by the elastic property of the deformable foot in the tangential direction. The parameters related to the normal and tangential forces are usually not equal. For example, in Figure 7, the normal force is primarily determined by the spring above the foot, while the tangential force is determined by the rubber pad mounted at the bottom of the foot.

3.2. Hard foot versus deformable terrain

If the foot is much harder than the terrain, the foot–terrain interaction mechanics is mainly determined by the properties and deformation of the soil. In the community of terramechanics, the mechanical properties of the terrain are usually divided into the bearing property in the normal direction and the shearing property in the tangential direction. The bearing property is characterized by a pressure–sinkage relationship, whereas the latter is characterized by a shear stress-displacement relationship.

The soil deforms under the vertical load, and the sinkage is composed of an elastic part and a plastic part with a complex transition area. As the theoretical prediction of the soil sinkage is difficult, plate-sinkage experiments are usually performed to characterize the bearing performance of the soil with semi-empirical equations. The most well-known pressure–sinkage models include those developed by Bernstein–Goriatchkin

$$\sigma(\delta) = k\delta^n, \tag{12}$$

Bekker

$$\sigma(\delta) = (k_c/b + k_\varphi)\delta^n, \tag{13}$$

and Reece (Wong 2008, 2009)

$$\sigma(\delta) = (ck'_c + \gamma_s b k'_\varphi)(\delta/b)^n, \tag{14}$$

The shearing stress can be predicted with the Janosi Formula (Janosi and Hanamoto, 1961):

$$\tau(j) = [c + \sigma \tan\varphi](1 - e^{-j/K}), \tag{15}$$

where σ (Pa) is the normal stress, τ (Pa) is the shearing stress, $k(\mathrm{Pa/m}^n)$ is the sinkage modulus of soil, δ is the soil deformation in the normal direction, $k_c(\mathrm{Pa/m}^{n+1})$ is the cohesive modulus of soil, b is the radius of the experimental plate, $k_\varphi(\mathrm{Pa/m}^n)$ is the frictional modulus of soil, c (Pa) is the cohesion of soil, $\varphi(^\circ)$ is the internal friction angle of soil, j (m) is the deformation of the soil in the tangential direction, and K(m)is the shearing deformation modulus of soil. Equations (13) and (14) have similar effects while predicting the normal force. Parameters k'_c and k'_φ are related to k_c and k_φ, respectively, and γ_s is the density of the soil. Equation (13) is adopted in this paper, as its parameters are more popular. Parameters for typical terrains are shown in Table 6 (Wong, 2008). Figures 8 shows the relationship of the normal stress versus soil deformation δ and that of the tangential stress versus soil deformation j. Suppose that $j > 0$ as a default while deducing the tangential force.

In order to deduce the foot–soil interaction models for different kinds of feet with the deformable terrain, the concept usually used in the community of terramechanics that decomposes the interaction stresses into the normal direction and tangential direction is adopted. Figure 9 shows the normal stress and the shearing stress that act on a flat foot by the deformable soil.

Table 6. Mechanical parameters for typical terrains (Wong, 2008).

Terrain	Moisture content (%)	n	k_c(kPa/m^{n-1})	k_φ(kPa/m^n)	c(kPa)	φ(°)
Dry sand (Land Locomotion Lab. LLL)	0	1.10	0.99	1,528.43	1.04	28.0
Sandy loam (LLL)	15	0.70	5.27	1,515.04	1.72	29.0
Sandy loam Michigan (Strong, Buchele)	23	0.40	11.42	808.96	9.65	35.0
Clayed soil (Thailand)	38	0.50	13.19	692.15	4.14	13.0
Heavy clay (Waterways Experiment Station, WES)	40	0.11	1.84	103.27	20.69	6.0
Upland sandy loam (Wong)	51	1.10	74.60	2,080.00	3.30	33.7
LETE sand (Wong)	–	0.79	102.00	5,301.00	1.30	31.1
Snow in the U.S. (Harrison)	–	1.60	4.37	196.72	1.03	19.7
Snow (Sweden)	–	1.44	10.55	66.08	6.00	20.7

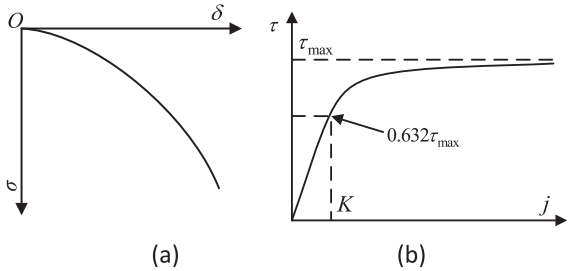

Fig. 8. Relationships of soil stresses and deformation: (a) σ versus δ; (b) τ versus j.

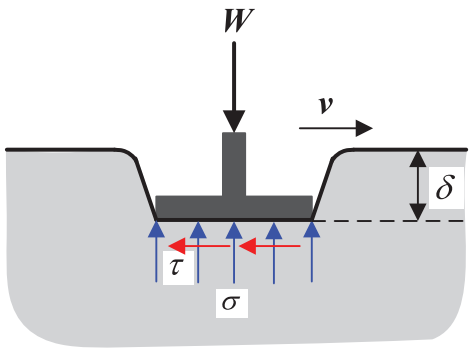

Fig. 9. Stress distribution under a flat foot.

Suppose that the normal stress is constant as is the shearing stress. According to Figure 9, the normal force and the tangential force are the integration of the normal stress and the shearing stress, respectively, and the results are

$$\begin{cases} F_{\mathrm{TN}} = \sigma S \\ F_{\mathrm{T}} = \tau S \end{cases}, \tag{16}$$

where S is the area of the foot that comes in contact with the terrain.

(1) *Flat circular foot*. For a flat circular foot with a radius of r, S in Equation (14) is πr^2; thus, the forces F_{N} and F_{T} are as follows:

$$\begin{aligned} F_{\mathrm{TN}} &= \pi r^2 (k_c/r + k_\varphi)\, \delta^n \\ &= (k_c \pi r + k_\varphi \pi r^2)\, \delta^n \end{aligned}, \tag{17}$$

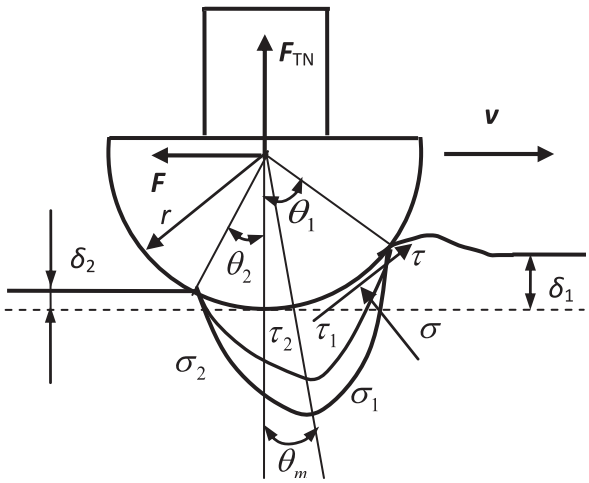

Fig. 10. Stress distribution under a cylindrical foot.

$$\begin{aligned} F_{\mathrm{T}} &= -\pi r^2 [c + \sigma \tan\varphi](1 - e^{-j/K}) \\ &= F_{\mathrm{TN}}(\pi r^2 c/F_{\mathrm{TN}} + \tan\varphi)(1 - e^{-j/K}) \end{aligned}. \tag{18}$$

(2) *Flat rectangular foot*. Substitute $S = ab$ into Equation (16); the mechanics for a flat rectangular foot with a width of b and a length of a is as follows:

$$\begin{cases} F_{\mathrm{TN}}(t) = (k_c a + k_\varphi ab)\, \delta^n \\ F_{\mathrm{T}} = F_{\mathrm{TN}}(abc/F_{\mathrm{TN}} + \tan\varphi)(1 - e^{-j/K}) \end{cases}. \tag{19}$$

(3) *Cylindrical foot*. If the foot is cylindrical, such as the foot of BigDog or ATHLETE, neither the normal stress nor the shearing stress is constant. Figure 10 shows the stress distribution under a cylindrical foot, where θ_1 and θ_2 are the entrance and leaving angles of the foot, respectively, θ_{m} is the angle at which the maximum normal stress and shearing stress occur, σ_1 and τ_1 represent the normal stress and shearing stress respectively (σ_1 and τ_1 represent the stresses from the angle θ_1 to θ_{m}, while σ_2 and τ_2 represent those from angle θ_{m} to θ_2).

The entry and exit angles are the functions of the soil deformation on both sides:

$$\theta_i = \arccos[(r - \delta_i)/r] \quad (i = 1, 2). \tag{20}$$

The normal stress can be calculated by the Wong–Reece model (Wong and Reece, 1967):

$$\begin{cases} \sigma_1(\theta)=(\frac{k_c}{b}+k_\varphi)r^n(\cos\theta-\cos\theta_1)^n & (\theta_m\le\theta\le\theta_1) \\ \sigma_2(\theta)=(\frac{k_c}{b}+k_\varphi)r^n\{\cos[\theta_1-\frac{\theta-\theta_2}{\theta_m-\theta_2}(\theta_1-\theta_m)]-\cos\theta_1\}^n & (\theta_2\le\theta<\theta_m) \end{cases} . \tag{21}$$

Substitute Equation (21) into Equation (15), the shearing stress is obtained. The stresses can be simplified into linearized equations (Shibly et al., 2005; Ding et al., 2009):

$$\begin{cases} \sigma_1(\theta)\approx\sigma_1^L(\theta)=\sigma_m(\theta_1-\theta)/(\theta_1-\theta_m) & (\theta_m\le\theta\le\theta_1) \\ \sigma_2(\theta)\approx\sigma_2^L(\theta)=\sigma_m(\theta-\theta_2)/(\theta_m-\theta_2) & (\theta_2\le\theta<\theta_m) \end{cases}, \tag{22}$$

$$\begin{cases} \tau_1(\theta)\approx\tau_1^L(\theta)=\tau_m(\theta_1-\theta)/(\theta_1-\theta_m) & (\theta_m\le\theta\le\theta_1) \\ \tau_2(\theta)\approx\tau_2^L(\theta)=\tau_m(\theta-\theta_2)/(\theta_m-\theta_2) & (\theta_2\le\theta<\theta_m) \end{cases} . \tag{23}$$

Note that the linearized equations are the approximated forms of the normal stress and tangential stress. Shibly et al. (2005) verified that this simplification is reasonable for several kinds of terrain.

The normal force and the tangential force are the integration of the stresses:

$$\begin{cases} F_{TN}=\int_{\theta_2}^{\theta_1}\int_{-b/2}^{b/2}[\sigma(\theta,b)\cos\theta+\tau(\theta,b)\sin\theta]r\mathrm{d}\theta\mathrm{d}y \\ F_T=\int_{\theta_2}^{\theta_1}\int_{-b/2}^{b/2}[-\sigma(\theta,b)\sin\theta+\tau(\theta,b)\cos\theta]r\mathrm{d}\theta\mathrm{d}y \end{cases} . \tag{24}$$

Substitute the stress equations into Equation (24); the closed-form equation is derived:

$$\begin{bmatrix} F_{TN} \\ F_T \end{bmatrix} = rb\begin{bmatrix} A & B \\ -B & A \end{bmatrix}\begin{bmatrix} \sigma_m \\ \tau_m \end{bmatrix}, \tag{25}$$

where

$$\begin{cases} A=\frac{\cos\theta_m-\cos\theta_2}{\theta_m-\theta_2}+\frac{\cos\theta_m-\cos\theta_1}{\theta_1-\theta_m} \\ B=\frac{\sin\theta_m-\sin\theta_2}{\theta_m-\theta_2}+\frac{\sin\theta_m-\sin\theta_1}{\theta_1-\theta_m} \\ \sigma_m=(k_c/b+k_\varphi)r^n(\cos\theta_m-\cos\theta_1)^n \\ \tau_m=(c+\sigma_m\tan\varphi)[1-e^{-j(\theta_m)/K}] \end{cases} .$$

Suppose that the terrain surface is flat and the normal stress is symmetric, i.e. $\theta_1=\theta_2$, $\theta_m=0$, and $\delta_1=\delta_2=\delta$; then, $A=2(1-\cos\theta_1)/\theta_1$, and $B=0$.

In order to understand the relationship of the forces and the soil deformation, Equation (25) should be simplified further. It is found that if θ_1 is smaller than $\pi/2$, the following equation is acceptable:

$$2(1-\cos\theta_1)\approx\theta_1^2. \tag{26}$$

Then,

$$2r(1-\cos\theta_1)=2\delta\approx r\theta_1^2. \tag{27}$$

Therefore,

$$A\approx\theta_1\approx\sqrt{2\delta/r}. \tag{28}$$

Substituting Equations (26)–(28) into Equation (25), one obtains the following:

$$F_{TN}=rbA\sigma_m=rb\sigma_m\cdot 2(1-\cos\theta_1)/\theta_1, \tag{29a}$$

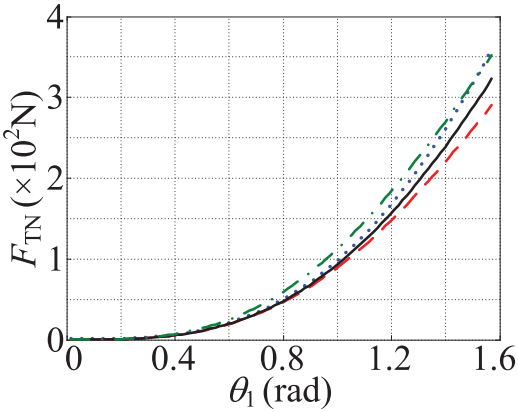

Fig. 11. Comparison of normal force with different models. The parameters are as follows: $r=0.05$m, $b=0.08$m, $n=1.10$, $k_c=990\,\mathrm{N/m^{n+1}}$, and $k_\varphi=1528430\,\mathrm{N/m^{n+2}}$. The dash-dotted line is the integrated equation $F_{TN}=2\int_0^{\theta_1}\sigma(\theta)\cos\theta\mathrm{d}\theta$ according to Equation (24); the dashed line is $F_{TN}=rb\cdot\sigma_m\cdot 2(1-\cos\theta_1)/\theta_1$ according to Equation (29a); the dotted line is according to Equation (29b); and the solid line is $F_{TN}=(\sqrt{2r}k_c+\sqrt{2r}bk_\varphi)\delta^{n+1/2}$ according to Equation (29c).)

$$F_{TN}\approx rb\theta_1\cdot\sigma_m=S\cdot\sigma_m/2, \tag{29b}$$

$$\begin{aligned} F_{TN}&\approx rb\sqrt{2\delta/r}\cdot(k_c/b+k_\varphi)\delta^n \\ &=(\sqrt{2r}k_c+\sqrt{2r}bk_\varphi)\delta^{n+1/2} \end{aligned} , \tag{29c}$$

$$\begin{aligned} F_T&=rbA\tau_m=rbA\cdot(c+\sigma_m\tan\varphi)\cdot(1-e^{-j/K}) \\ &\approx(rb\theta_1c+F_{TN}\tan\varphi)\cdot(1-e^{-j/K}) \\ &\approx F_{TN}(\sqrt{2r\delta}bc/F_{TN}+\tan\varphi)\cdot(1-e^{-j/K}) \end{aligned} . \tag{30}$$

Figure 11 verifies that the simplified models of F_N in Equation (29) are reasonable. The maximum errors of Equations (29a), (29b) and (29c) comparing with the integrated results obtained by Equation (24) are 17.5%, 4.9%, and 8.8%, respectively. The contact area increases with the wheel sinkage, and it is approximately proportional to $\delta^{1/2}$; the maximum normal stress is proportional to δ^n; therefore, the normal force is proportional to $\delta^{n+1/2}$. In Equation (29b), the parameter $S=2rb\theta_1$, which denotes the contact area of the cylindrical foot with the soil. According to Equations (29c) and (30), the sinkage exponent for the cylindrical feet is mainly determined by the soil's property. However, the other equivalent parameters, including the rigidity coefficient $\sqrt{2r}k_c+\sqrt{2r}bk_\varphi$ and the frictional coefficient $(\sqrt{2r\delta}bc/F_{TN}+\tan\varphi)\cdot(1-e^{-j/K})$, are the functions of not only the terrain property parameters P_T, but also the feet parameters P_F and the motion state variables P_M.

(4) *Spherical foot*. The stress distribution under a spherical foot is shown in Figure 12.

Suppose that $\theta_m=0$ and the stress distribution is symmetrical; then, the normal force is as follows:

$$F_{TN}=\int_{\theta_m}^{\theta_1}R\cos\theta\sigma(\theta)\mathrm{d}\theta\int_0^{2\pi}R\sin\theta\mathrm{d}\varphi. \tag{31}$$

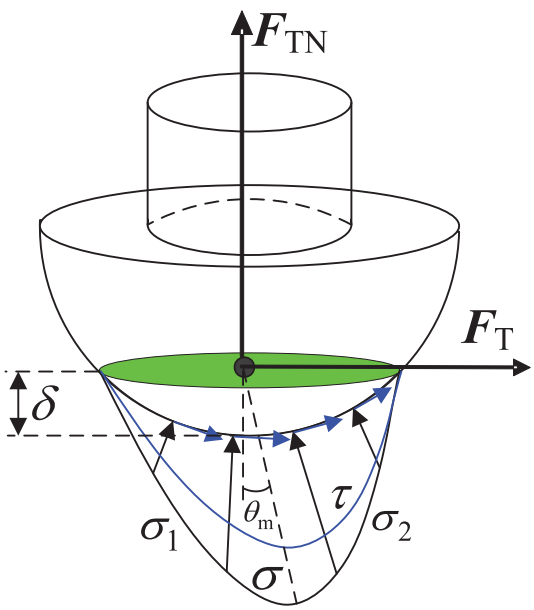

Fig. 12. Stress distribution under a spherical foot.

Substituting $\sigma(\theta)=\sigma_m(\theta_1-\theta)/(\theta_1-\theta_m)$ (Shibly et al., 2005; Ding et al., 2009) into Equation (31), where $\sigma_m=(k_c/R+k_\varphi)\delta^n$, one obtains the following:

$$F_{TN}=\pi R^2\int_{\theta_m}^{\theta_1}\sigma_m(\theta_1-\theta)/(\theta_1-\theta_m)\sin(2\theta)\,d\theta$$
$$=\pi R^2\sigma_m\left[\cos(2\theta_m)-\frac{\sin(2\theta_1)-\sin(2\theta_m)}{2(\theta_1-\theta_m)}\right]. \quad (32)$$

Consider that $\theta_m=0$; then, the simplified form of Equation (32) is as follows:

$$F_{TN}=\pi R^2\sigma_m\left(1-\frac{\sin\theta_1\cos\theta_1}{\theta_1}\right). \quad (33)$$

If θ_1 is small, $\sin\theta_1\approx\theta_1$, and one has the following:

$$F_{TN}\approx\pi R\delta\sigma_m=(\pi k_c+\pi Rk_\varphi)\delta^{n+1}. \quad (34)$$

Figure 13 verifies that the approximation Equation (34) of normal force F_N is close to that predicted by Equation (33) if θ_1 is not larger than $\pi/2$.

The contact area S of a spherical cap with a height of δ is $2\pi R\delta$. Hence, the normal force F_N is also equal to $S\sigma_m/2$ approximately, the same as the normal force of the cylindrical foot.

The tangential force is as follows:

$$F_T=\int_{\theta_m}^{\theta_1}R\cos\theta\tau(\theta)\,d\theta\int_0^{2\pi}R\sin\theta\,d\varphi$$
$$=\pi R^2\tau_m\left(1-\frac{\sin\theta_1\cos\theta_1}{\theta_1}\right)\approx\pi R\delta\tau_m$$
$$=\pi R\delta(c+\sigma\tan\varphi)(1-e^{-j/K}) \quad (35)$$
$$=F_{TN}(\pi R\delta c/F_{TN}+\tan\varphi)(1-e^{-j/K}).$$

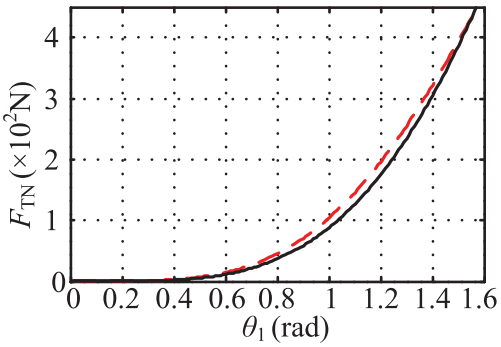

Fig. 13. Comparison of predicted normal force for a spherical foot. The parameters are the same as those in Figure 11. The solid line is $F_{TN}=\pi R^2\sigma_m[1-(\sin\theta_1\cos\theta_1)/\theta_1]$, and the dashed line is $F_{TN}=(\pi k_c+\pi Rk_\varphi)\delta^{n+1}$.

The interaction force of several types of feet and the deformable terrain is derived. In order to generalize the equations and disclose the relationship between the conventional contact models and the terramechanics-based models, some further analysis should be performed.

(1) *Normal force*. If the bottom of a foot is flat, the normal stress under it can be considered constant, and the normal force is the product of the foot's bottom area S and the normal stress σ, which is the function of the soil deformation δ according to Bekker's model in Equation (13). For the cylindrical foot and the spherical foot, the normal stress under them can be predicted by the Wong–Reece model and then linearized. The normal force is approximately equal to $S\sigma_m/2$, where σ_m denotes the normal stress at the maximum stress angle θ_m and S denotes the contact area of a foot with the soil.

Equations (17), (19), (29), and (34) can predict the normal forces that act on the flat circular foot, flat rectangular foot, spherical foot, and spherical foot, respectively, by the deformable soil. As the damping term is not considered, the equations have the same form as Hertz's model $F_{TN}=k_{TN}\delta^{n_{TN}}$. Table 7 shows the rigidity parameters k_{TN} for different feet. Not only are parameters k_{TN} the functions of the soil's mechanical property parameters but they are also related to the feet's parameters and shape, despite that the normal force is primarily generated by the deformation of the soil. The parameter n_{TN} is the function of the soil's sinkage exponent n and the feet's shape. If a foot is flat, n_{TN} is equal to n, whereas n_{TN} are $n+1/2$ and $n+1$ for a cylindrical foot and a spherical foot, respectively. Note that the soil deformation δ is usually smaller than 1 m, so the normal force is the decreasing function of parameter n_{TN}. If the vertical load that should be balanced by the normal force is given and the parameters k_{TN} for different feet are the same, the soil deformation for the flat foot is the smallest and that for the spherical foot is the largest.

If the normal stresses are not symmetrical, the parameters of Hertz's model are influenced. A reasonable assumption for the cylindrical and the spherical feet is that only the side

that squeezes the soil has stresses and the other side has no stress; then, the parameter k_{TN} becomes a half of the values in Table 7, and the parameters n_{TN} are not influenced.

(2) *Tangential force*. Equations for predicting the tangential force of the flat circular foot, flat rectangular foot, rectangular foot, and spherical foot are shown by Equations (18), (19), (30), and (35), respectively. If the soil deformation j is larger than zero, the form of tangential force F_H is as follows:

$$F_{\mathrm{H}} = \mu F_{\mathrm{TN}}(1 - e^{-j/K}). \tag{36}$$

If $j < 0$, the term $1 - \mathrm{e}^{-j/K}$ should be $-(1 - \mathrm{e}^{j/K})$. Considering the direction of the foot's motion, a combination of the tangential force is as follows:

$$F_{\mathrm{H}} = -\mu F_{\mathrm{TN}} \mathrm{sgn}(j)(1 - \mathrm{e}^{-|j|/K}), \tag{37}$$

where

$$\mathrm{sgn}(j) = \begin{cases} 1 & (j > 0) \\ 0 & (j = 0) \\ -1 & (j < 0) \end{cases}. \tag{38}$$

In order to understand the relationship of Equation (37) and the conventional friction models, the following simplification is made:

$$\mathrm{sgn}(j)(1 - \mathrm{e}^{-|j|/K}) \approx \begin{cases} j/(2K) & (|j| \le 2K) \\ 1 & (|j| > 2K) \end{cases}. \tag{39}$$

Figure 14 verifies the reasonability $1 - e^{-j/K}$ and the simplification results of Equation (37) when $j > 0$. Then, the tangential force F_{H} is as follows:

$$F_{\mathrm{H}} \approx \begin{cases} \mu F_{\mathrm{TN}} \cdot j/(2K) & (|j| \le 2K) \\ \mu F_{\mathrm{TN}}\ \mathrm{sgn}(j) & (|j| > 2K) \end{cases}. \tag{40}$$

On comparing Equation (40) with Equations (10) and (11), some obvious distinctions can be found. First, the tangential force depends on the soil deformation in the horizontal plane rather than on the velocity. If the soil deformation is larger than $2K$, the absolute value of the horizontal force is μF_{TN}, whereas such a value is obtained immediately when the velocity is not zero in the conventional model. Second, the friction coefficient μ is not a constant value determined by the properties of the soil and the foot material any longer. The parameter μ has two components: one is tan φ, the tangential function of the soil's internal angle, and the other is the function of the soil's internal cohesion c. The maximum tangential force caused by the internal cohesion of the soil is approximately proportional to the product of c and the contact area S. If the component related to c is considered as a part of the friction coefficient, it should be divided by the normal force F_{N}. Third, Hertz's model can also be used to predict the horizontal force if j is smaller than $2K$:

$$F_{\mathrm{H}} = \begin{cases} \mathrm{sgn}(j) k_{\mathrm{TT}} |j|^{n_{\mathrm{TT}}} & (|j| \le 2K) \\ \mathrm{sgn}(j) \mu F_{\mathrm{N}} & (|j| > 2K) \end{cases}. \tag{41}$$

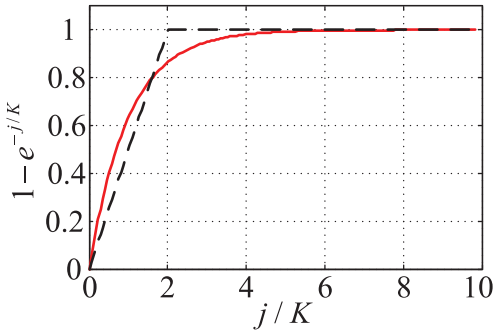

Fig. 14. Plot of $1 - e^{-j/K}$ and its simplification result versus j/K.

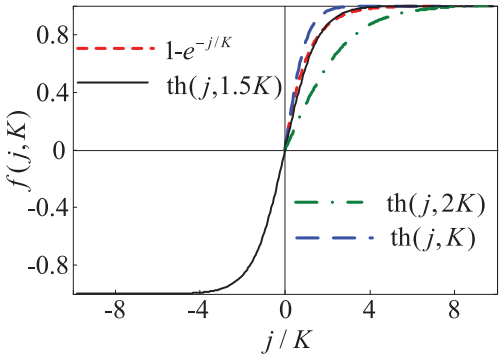

Fig. 15. Comparison of $1 - e^{-j/K}$ and th$(\cdot)$ functions.

The parameter k_{TT} is the function of the friction coefficient. Table 7 also shows the parameters μ, k_{TT}, and n_{TT}.

Equation (37) includes a signal function, and the first-order derivative of Equation (40) is not continuous. In order to express the tangential force with a smooth function, the hyperbolic tangent function is adopted:

$$\mathrm{th}(j, K') = \frac{e^{j/K'} - e^{-j/K'}}{e^{j/K'} + e^{-j/K'}}. \tag{42}$$

It is found that the function $\mathrm{sgn}(j)(1 - \mathrm{e}^{-|j|/K})$ can be replaced by the function $\mathrm{th}(j, K')$ with a small error if K' is equal to $1.5K$, i.e.

$$\mathrm{sgn}(j)(1 - \mathrm{e}^{-|j|/K}) \approx \mathrm{th}(j, 1.5K). \tag{43}$$

Figure 15 compares the curves of $(1 - \mathrm{e}^{-j/K})$, th(j, K), th$(j, 1.5K)$, as well as th$(j, 2K)$. It is obvious that the curve of $(1 - \mathrm{e}^{-j/K})$ is among those of th(j, K) and th$(j, 2K)$, and the curves of $(1 - \mathrm{e}^{-j/K})$ and th$(j, 1.5K)$ are quite close to each other.

As a result, the horizontal force can be simplified as follows:

$$F_{\mathrm{H}} = -\mathrm{th}(j, 1.5K)\, \mu F_{\mathrm{TN}}. \tag{44}$$

3.3. Deformable foot versus deformable terrain

If both the foot and the terrain are deformable, the situation will be much complex. It is actually a two-degree-of-freedom (2-DOF) dynamic system, as shown in Figure 6.

If the foot and the terrain are considered as a whole, the normal force that acts on the robot is as follows:

$$F_{\mathrm{N}} = k_{\mathrm{N}}\delta^{n_{\mathrm{N}}} + b_{\mathrm{N}}\delta^{p_{\mathrm{N}}}\dot{\delta}^{q_{\mathrm{N}}} \tag{45}$$

where $\delta = \delta_{\mathrm{F}} + \delta_{\mathrm{T}}$ is the summation of the foot deformation and the terrain deformation and k_N, b_N, n_N, p_N, and q_N are the equivalent parameters considering both the foot and the terrain. One should determine the unknown parameters in Equation (45) before it could be used.

The forces of the foot–terrain system caused by the terrain and the foot are denoted by F_{TN} and F_{FN}, respectively, the equations of which are

$$\begin{cases} F_{\mathrm{TN}} = k_{\mathrm{TN}}\delta_{\mathrm{T}}^{n_{\mathrm{TN}}} + b_{\mathrm{TN}}\delta_{\mathrm{T}}^{p_{\mathrm{TN}}}\dot{\delta}_{\mathrm{T}}^{q_{\mathrm{TN}}} \\ F_{\mathrm{N}}{=}F_{\mathrm{FN}} = k_{\mathrm{FN}}\delta_{\mathrm{F}}^{n_{\mathrm{FN}}} + b_{\mathrm{FN}}\delta_{\mathrm{F}}^{p_{\mathrm{FN}}}\dot{\delta}_{\mathrm{F}}^{q_{\mathrm{FN}}} \end{cases} . \tag{46}$$

The dynamics model of the 2-DOF foot–terrain system is as follows:

$$\begin{cases} k_{\mathrm{FN}}\delta_{\mathrm{F}}^{n_{\mathrm{FN}}} + b_{\mathrm{FN}}\delta_{\mathrm{F}}^{p_{\mathrm{FN}}}\dot{\delta}_{\mathrm{F}}^{q_{\mathrm{FN}}}{=}W - M\ddot{\delta} \\ k_{\mathrm{TN}}\delta_{\mathrm{T}}^{n_{\mathrm{TN}}} + b_{\mathrm{TN}}\delta_{\mathrm{T}}^{p_{\mathrm{TN}}}\dot{\delta}_{\mathrm{T}}^{q_{\mathrm{TN}}} - m_{\mathrm{F}}g + m_F\ddot{\delta}_{\mathrm{T}} = \\ k_{\mathrm{FN}}\delta_{\mathrm{F}}^{n_{\mathrm{FN}}} + b_{\mathrm{FN}}\delta_{\mathrm{F}}^{p_{\mathrm{FN}}}\dot{\delta}_{\mathrm{F}}^{q_{\mathrm{FN}}} \end{cases} . \tag{47}$$

The dynamics model includes two nonlinear oscillation equations with two state variables. It is not easy to obtain the parameters in Equation (45) by solving Equations (46) and (47), although the approximate equivalent parameters could be solved using the theory of nonlinear oscillation (Nayfeh and Mook, 2004). For simplification, considering the static state of the foot–terrain interaction, one obtains the following:

$$\begin{cases} W = k_{\mathrm{FN}}\delta_{\mathrm{F}}^{n_{\mathrm{FN}}} \\ W + m_{\mathrm{F}}g = k_{\mathrm{TN}}\delta_{\mathrm{T}}^{n_{\mathrm{TN}}} \end{cases} . \tag{48}$$

Solving Equation (48), one obtains the following:

$$\begin{cases} \delta_{\mathrm{F}} = \sqrt[n_{\mathrm{FN}}]{W/k_{\mathrm{FN}}} \\ \delta_{\mathrm{T}} = \sqrt[n_{\mathrm{TN}}]{(W + m_{\mathrm{F}}g)/k_{\mathrm{TN}}} \end{cases} . \tag{49}$$

Combining Equation (45) with Equation (49), one obtains the following:

$$k_{\mathrm{N}}\delta^{n_{\mathrm{N}}} = W = k_{\mathrm{N}}\left(\sqrt[n_{\mathrm{FN}}]{W/k_{\mathrm{FN}}} + \sqrt[n_{\mathrm{TN}}]{(W + m_{\mathrm{F}}g)/k_{\mathrm{TN}}}\right)^{n_{\mathrm{N}}}, \tag{50}$$

$$k_{\mathrm{N}} = \frac{W}{\left[\left(\sqrt[n_{\mathrm{FN}}]{\frac{W}{k_{\mathrm{FN}}}} + \sqrt[n_{\mathrm{TN}}]{\frac{W+m_{\mathrm{F}}g}{k_{\mathrm{TN}}}}\right)\right]^{n_{\mathrm{N}}}}. \tag{51}$$

From Equation (51), one knows that the equivalent rigidity coefficient k_{N} is the function of the equivalent exponent n_{N}. Even if n_{N} is supposed to be 1 and the gravity of the foot is neglected, the following equation shows that k_{N} is still influenced by the vertical load W, which is caused by the nonlinear characteristics of the foot and the soil:

$$k_{\mathrm{N}} = \frac{\sqrt[n_{\mathrm{FN}}]{k_{\mathrm{FN}}}\,\sqrt[n_{\mathrm{TN}}]{k_{\mathrm{TN}}}\,W}{\sqrt[n_{\mathrm{FN}}]{W^{1-n_{\mathrm{FN}}}}\,\sqrt[n_{\mathrm{TN}}]{k_{\mathrm{TN}}} + \sqrt[n_{\mathrm{TN}}]{W^{1-n_{\mathrm{TN}}}}\,\sqrt[n_{\mathrm{FN}}]{k_{\mathrm{FN}}}}. \tag{52}$$

Equations (48)–(52) show that even for the static state, the equivalent rigidity coefficient and exponent are not easy to determine. As it is not easy to calculate the equivalent parameters, two alternative approaches can be used for analyzing the interaction mechanics of a deformable foot on the deformable soil. (1) Take the foot–soil system as a whole, and identify the parameters in Equation (45) directly by considering the properties of the foot and the soil as the black box. (2) Consider the deformable foot and the deformable soil as a 2-DOF system, and identify two groups of parameters in Equation (46). The disadvantage of the second approach is that it needs to determine two groups of parameters; however, the parameters are meaningful, and some of them can be predicted theoretically.

Remark 1. The interaction mechanics of the foot and terrain studied in this paper is quasi-static with modest velocity. The terradynamics of legged locomotion that considers the dynamics of terrain is much more complicated and requires further study (Li et al., 2013). The tangential force experiments introduced in Section 5 used horizontal velocities of ±20 mm/s. The model requires that the entrance angle of the foot be less than $\pi/2$ so that the model will not violate Equation (29). The bulldozing phenomenon has not been considered explicitly in the model. Errors of the model could be reduced by appropriate parameter identification.

4. Standard dynamic model and parameter identification method

In Section 3, the absolute values of the forces and the motion state variables are the main concern, and their signals are not considered explicitly. In order to support the dynamics simulation and the real-time control of legged robots, the standard dynamic model and the parameter identification method should be developed. The standard dynamic model considers the contact process as a function of time, and the signals of forces are explicitly included with the position and velocity of the foot in a unified coordinate.

4.1. Standard dynamic model

At the very time that the foot comes into contact with the terrain, the local coordinate *O-xz* of the foot is established, as shown in Figure 6, and the time t is set to be zero. For the reason of simplification, the direction of the coordinate axis x is set to be the same as that of the foot's tangential velocity, and the axis z is normal to the terrain. If it is for simulation, the contact can be checked by a geometric calculation. During the process of control, the contact can be found by a force sensor. The force acting point, which is denoted by P, attaches to the foot and moves with it while

Table 7. Parameters for different feet with symmetrical stress distribution.

Model name	k_{TN}	n_{TN}	μ	k_{TT}	n_{TT}
Flat circular	$k_c\pi r + k_\varphi \pi r^2$	n	$\pi r^2 c/F_{\mathrm{TN}} + \tan\varphi$	$\mu F_{\mathrm{N}}/(2K)$	1
Flat rectangular	$k_c a + k_\varphi ab$	n	$abc/F_{\mathrm{TN}} + \tan\varphi$	$\mu F_{\mathrm{N}}/(2K)$	1
Cylindrical	$\sqrt{2r}k_c + \sqrt{2r}bk_\varphi$	n+1/2	$\sqrt{2r}bc/[\sqrt[(2n+1)]{(\sqrt{2r}k_c + \sqrt{2r}bk_\varphi)F_{\mathrm{TN}}^{2n}}] + \tan\varphi$	$\mu F_{\mathrm{N}}/(2K)$	1
Spherical	$\pi k_c + \pi R k_\varphi$	n+1	$\pi Rc/[\sqrt[n+1]{(\pi k_c + \pi R k_\varphi)F_{\mathrm{TN}}^{n}}] + \tan\varphi$	$\mu F_{\mathrm{N}}/(2K)$	1

the deformation occurs, but point O keeps still in the inertial coordinate during the process of a contact. At time t, the coordinates of point P are $x(t)$ and $z(t)$.

The normal force FN for the feet and the terrain with different properties is as follows:

$$F_{i\mathrm{N}} = \begin{cases} 0 & (z > 0) \\ -\mathrm{sgn}(z(t))\, k_{i\mathrm{N}} |z(t) - z(0)|^{n_{i\mathrm{N}}} & \\ -\mathrm{sgn}(\dot{z}(t))\, b_{i\mathrm{N}} |z(t) - z(0)|^{p_{i\mathrm{N}}} |\dot{z}(t)|^{q_{i\mathrm{N}}} & (z < 0) \end{cases}, \tag{53}$$

where i stands for F (foot) if the foot is deformable and the terrain is hard, stands for T (terrain) if the terrain is deformable and the foot is hard, and stands for nothing if both the terrain and the foot are deformable.

If the soil is deformable, its hysteresis phenomena should be considered. Experiments show that the compressing process of the contact force in the normal direction can be predicted with Equation (55). However, the force F_{TN} turns to zero abruptly when the foot begins to leave the soil, i.e. immediately when $\dot{z}(t) > 0$. It means that the plastic deformation of the soil causes severe hysteresis on the normal force that acts on the foot by the soil. Equation (53) should be improved for a hard foot on the deformable soil with large hysteresis when $z(t) - z(0) \le 0$ and $\dot{z}(t) \ge 0$:

$$F_{\mathrm{TN}} = W + m_{\mathrm{F}}\mathrm{g} \quad (z(t) - z(0) \le 0 \text{ and } \dot{z}(t) \ge 0). \tag{54}$$

The equation for predicting tangential force F_{T} is as follows:

$$F_{\mathrm{T}} = \begin{cases} -\mathrm{sgn}(x(t))\, k_{i\mathrm{T}} |x(t) - x(0)|^{n_{\mathrm{FT}}} & \\ -\mathrm{sgn}(\dot{x}(t))\, b_{i\mathrm{T}} |x(t) - x(0)|^{p_{i\mathrm{T}}} |\dot{x}(t)|^{q_{i\mathrm{T}}} & \\ (|F_{\mathrm{T}}| \le \mu F_{\mathrm{TN}}) & \\ -\mu F_{\mathrm{TN}} \mathrm{sgn}(\dot{x}(t)) & (\text{Otherwise}) \end{cases}. \tag{55}$$

For the hard foot and the deformable terrain, substitute the related parameters deduced in Section 3 into Equation (55); the following particular form of the tangential force is obtained:

$$\begin{aligned} F_{\mathrm{T}} &= -\mathrm{sgn}(x(t) - x(0))\,(1 - \mathrm{e}^{-|x(t)-x(0)|/K})\,\mu F_{\mathrm{TN}} \\ &\approx -\mathrm{th}(x(t) - x(0), 1.5K)\,\mu F_{\mathrm{TN}} \end{aligned}. \tag{56}$$

4.2. Parameter identification method

The parameters from Equations (53)–(56) should be identified. Equations (53) and (55) have the form of the Hunt–Crossley model, each including five unknown parameters. Equation (55) has two unknown parameters that need to be identified. The parameter identification methods of the normal force model, i.e. Equation (53), and the tangential force model, i.e. Equation (55), will be investigated as examples.

For the normal force model, it is hard to identify the parameters with a single experiment. Instead, it is feasible to identify the parameters by dividing them into two groups: one group includes the static parameters, i.e. the rigidity parameter k and the exponent n, and the other group includes the dynamic damping parameters, i.e. b, p, and q.

Define the 2-norm as follows:

$$\|F(x, xdata) - ydata\|_2^2 = \sum_{i=1}^{m} [F(x, xdata_i) - ydata_i]^2. \tag{57}$$

The parameter identification process is to find the optimal values of x to minimize the 2-norm of the vector of prediction errors: $F(x, xdata) - ydata$.

The parameters of k and n can be identified by the data of the static state experiments. Exert an increasing vertical load on the foot at a very low speed, and sample the data of the normal force and the deformation. The parameters k and n can be obtained by finding the optimal values to satisfy the following equation:

$$\min_{\{k,n\}} \sum_{i=1}^{m} [-\mathrm{sgn}(z(t_i))\, k\, |z(t_i) - z(0)|^n - F_{\mathrm{N}}(t_i)]^2, \tag{58}$$

where t_i is the ith sampling time and m is the overall sampling time.

Also, k and n can be identified using the deformation and the sinkage obtained at the static state of the experiments with different vertical loads:

$$\min_{\{k,n\}} \sum_{j=1}^{m'} [-\mathrm{sgn}(z(t_{ej}))\, k\, |z(t_{ej}) - z(0)|^n - F_{\mathrm{N}}(t_{ej})]^2, \tag{59}$$

where $z(t_{ej})$ is the static sinkage at the end of the jth experiment and m' is the times of experiment.

The other three parameters can only be identified using the dynamic process of the foot–terrain interaction. Parameters b, p, and q can be identified by searching their optimal values to satisfy the following equation:

$$\begin{aligned} \min_{\{b,p,q\}} \textstyle\sum_{i=1}^{m} [&-\mathrm{sgn}(z(t_i) - z(t_0))\, \hat{k}\, |z(t_i)|^{\hat{n}} - \mathrm{sgn}(\dot{z}(t_i)) \times \\ &b\, |z(t_i) - z(t_0)|^p\, |\dot{z}(t_i)|^q - F_{\mathrm{N}}(t_i)]^2 \end{aligned}. \tag{60}$$

As for the tangential force models, the parameters μ and K can be identified using the friction experiment by searching for the optimal values to satisfy the following equation:

$$\min_{\{\mu,K\}} \sum_{i=1}^{m} [-\mathrm{sgn}(x(t)-x(0))\cdot \mu F_{\mathrm{TN}}(1-e^{-|x(t_i)-x(0)|/K}) - F_{\mathrm{H}}(t_i)]^2$$

or

$$\min_{\{\mu,K\}} \sum_{i=1}^{m} [-\mathrm{th}(x(t_i)-x(0), 1.5K)\,\mu F_{\mathrm{TN}} - F_{\mathrm{H}}(t_i)]^2. \quad (61)$$

For the deformable soil, the frictional coefficient μ is the function of soil parameters and is influenced by the normal force; thus, the soil parameters can be further identified as follows.

If one wants to identify the parameters c and φ, μF_{TN} in Eqs.uations (61) and (62) should be substituted by $Sc + \tan\varphi F_{\mathrm{TN}}$ for flat feet and $Sc/2 + \tan\varphi F_{\mathrm{TN}}$ for cylindrical or spherical feet, where S is $\pi r^2, \pi ab, b\sqrt{2r(z(t)-z(0))}$, and $2\pi R(z(t)-z(0))$, respectively. For instance, for the spherical foot, the parameters of the terrain can be identified as follows:

$$\min_{\{c,\mu,K\}} \frac{1}{2} \sum_{i=1}^{m} [-\mathrm{sgn}(x(t_i)-x(0))\cdot bc\sqrt{2r(z(t_i)-z(0))} + F_{\mathrm{TN}}(t_i)\tan\varphi)(1-e^{-|x(t_i)-x(0)|/K}) - F_{\mathrm{H}}(t_i)]^2. \quad (62)$$

A simulation was carried out according to Equation (47) to verify the parameter identification method. The Hunt–Crossley model parameters for the deformable foot are as follows: k = 10,000 $\mathrm{Nm}^{-1.3}$, b = 500 $\mathrm{Nm}^{-1.4}\,\mathrm{s}^{1.1}$, n = 1.3, p = 0.3, and q = 1.1. The terrain is hard with no deformation. The parameters in Equation (47) are as follows: $M = 30$ kg, $W = 294$ N, and $m_{\mathrm{F}} = 0$. The fminsearch() function in Matlab is used to realize the parameter identification with Equation (60), which finds the minimum of a scalar function of several variables, starting at an initial estimate, referred to as the unconstrained nonlinear optimization. Equation (60) can obtain the original values of parameters of n, p, and q using the data obtained from the simulation. The reversibility of the simulation and the parameter identification is verified. In order to investigate the influence of the measured errors on the identified parameters, the normal force is measured with a noise added to the original value in the range from –10 to 10 N, generated by the random() function in Matlab. The original normal force and the measured results with noise during the simulation are shown in Figure 16. The identified parameters are as follows: $\hat{b} = 413.97$, $\hat{p} = 0.21$, and $\hat{q} = 1.15$.

Define the relative error of identified parameters:

$$Err = \frac{x - \hat{x}}{x} \times 100\%, \quad (63)$$

where x represents the unknown parameters and $\hat{x}$ represents the identified parameters. The relative errors of the identified parameters are 17.2%, 30.0%, and 4.5%, respectively.

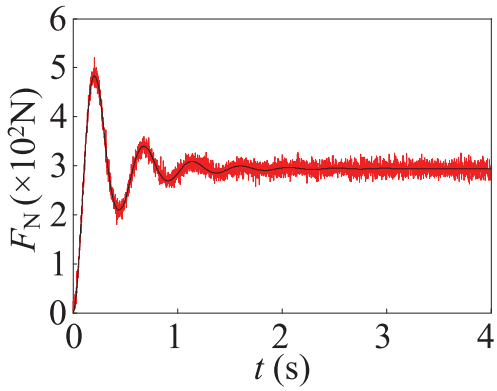

Fig. 16. Original normal force and measured results with noise during simulation.

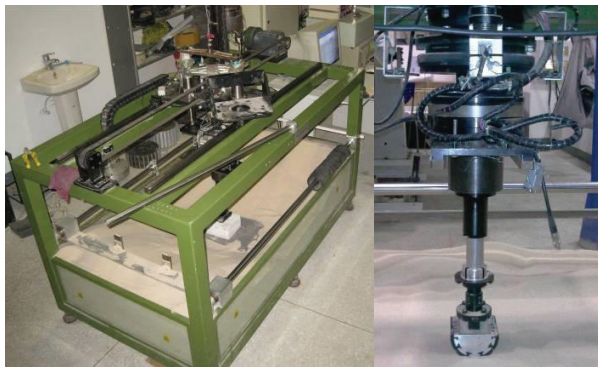

Fig. 17. Testbed for measuring foot–terrain interaction mechanics.

Define the relative error of the predicted results using the identified parameters as

$$Err = \frac{ydata_i - F(\hat{x}, xdata_i)}{\max|ydata_i|}. \quad (64)$$

The maximum absolute values of the relative errors for foot sinkage, normal force, and velocity are 2.62%, 2.05%, and 3.31%, respectively. The errors of the predicted results using the identified parameters are much smaller, although the parameter identification errors are a bit large. The differences in the original and identified parameters have little influence on the dynamic process of the foot–terrain interaction.

5. Experimental verification

5.1. Experimental setup

The wheel–soil interaction testbed developed in the Chinese State Key Laboratory of Robotics and Systems of Harbin Institute of Technology (Ding et al., 2011b; Song, 2012), as shown in Figure 17, was altered to test the foot–soil interaction mechanics. The displacement sensor on the testbed is

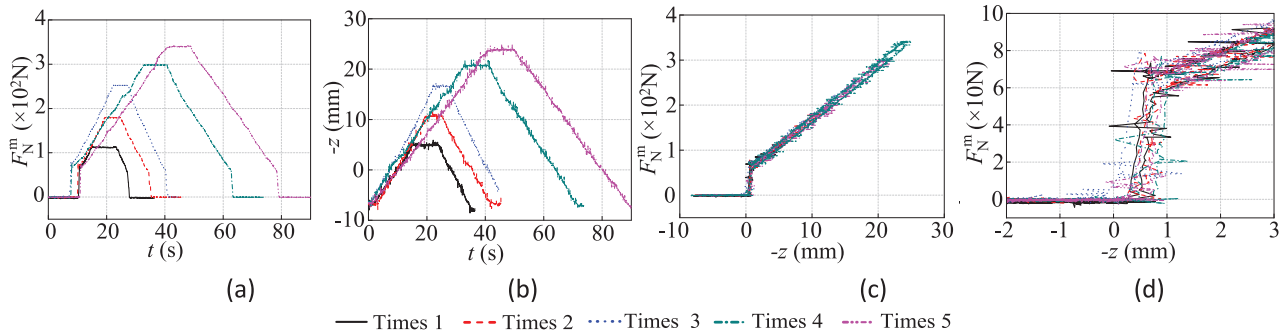

Fig. 18. Original quasi-static loading experimental results of deformable foot versus hard terrain (Group 1): (a) F_N^m versus t; (b) z versus t; (c) F_N^m versus z; (d) F_N^m versus z (enlarged).

used to measure the deformation of the foot and the terrain, and the foot is mounted on the six-axis F/T sensor, which is used to measure the normal force and tangential force that act on the foot by the terrain. The carriage motor is used together with a conveyance belt that drags the foot to move forward, in order to test the tangential force.

The foot of a four-legged robot is used to test the interaction mechanics with the terrain, as shown in Figure 17. The radius of the cylindrical foot is 0.05 m, and its width is 0.08 m. A rubber pad is mounted at its bottom. A spring can be mounted to make the foot a deformable foot, and it will be hard (neglecting the deformation of the rubber pad) if the spring is removed.

Different kinds of terrain are used. A kind of commercial standard sand is used to form the deformable terrain. The flat hard terrain is made from three different kinds of materials: brick, marble, and steel.

Experiments were carried out to test the normal force and the tangential force, respectively. In the normal direction, two kinds of experiments are carried out: (1) quasi-static loading and (2) loading with impact. In the quasi-static loading experiment, the jack that sustains the foot and the weight above it is controlled to move with a very low velocity. The foot moves downward slowly and then comes into contact with the terrain. A while after the foot arrives at its lowest position, it is controlled to move upwards slowly until the foot leaves the terrain. During the loading with impact experiments, the foot moves down freely from a certain height in order to measure the interaction mechanics including damping. Different vertical loads are set in order to investigate their influence. The most commonly used vertical loads are 100, 200, 250, 300, and 350 N. The tangential force experiments were carried out by controlling the foot to move with a horizontal velocity of 20 or –20 mm/s. The experimental description, group number, test number, vertical load, properties of the foot and the terrain, and initial height are tabulated in Table 8.

The normal force, tangential force, and vertical coordinates of the foot are acquired at a sampling frequency of 50 Hz. The experiments with the same condition are performed for more than five times to ensure the repeatability and effectiveness of the experimental results.

Let F_N^m denote the measured force by the F/T sensor above the foot. As the F/T sensor is calibrated and the data are set to be zero when the foot with a gravity of $m_F g$ is suspended from it, one has the following:

$$F_N^m = F_N + m_F g. \tag{65}$$

The sinkage, which is denoted by z, is set to zero when the foot just contacts with the terrain, and it is negative when the foot enters into the soil. So that $-z$ is used, in order draw the figures with positive values. The tangential deformation of the soil, denoted by j, is zero before the horizontal motion occurs; it is positive when the foot is dragged to move to the left side, and it is negative when the foot moves to the right side.

5.2. *Deformable foot versus hard terrain*

For the contact of the deformable foot with the hard terrain, the normal force F_N is equal to F_{FN}, which is generated by the spring on the foot, and

$$F_N = F_{FN} = F_N^m - m_F g. \tag{66}$$

Figure 18 shows the original quasi-static loading experimental data of experiments for the deformable foot versus the hard terrain. During the experiments, the measured force and the foot sinkage increase, remain steady, and then decrease. The measured normal force increases linearly with the increment of the wheel sinkage according to Figure 18(c). Figure 18(d) shows the enlarged figure of the time when the foot just comes into contact with the terrain. The contact force increases abruptly from zero to approximately 50 N ($m_F g$) to balance the gravity of the foot, and the increment of the foot sinkage is about 0.5 mm. This means that the rigidity of the foot pad, which balances the weight of the foot, is about 105 N/m. Then, the spring begins to deform and generate a linearly increasing force. The rigidity of the pad is much larger than that of the spring. So, the deformation of the pad is ignored.

The steady values of the measured normal force and the foot sinkage, as well as their average values, are listed

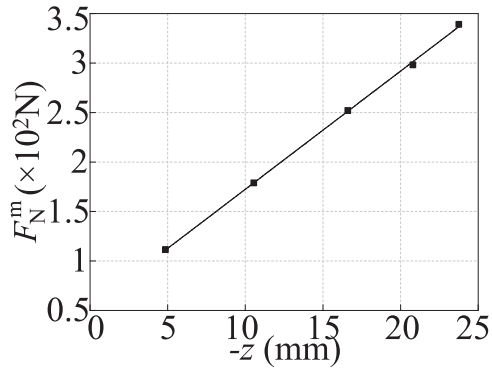

Fig. 19. Data fitting results using the average values in Table 10.

in Table 9. The parameters are identified with the linear regression approach using the average values of $F_N m$ and z according to Equation (61). The identified results of the parameters are as follows: $k_{FN} = 1.194 \times 104\,\mathrm{N/m}$, $n_{FN} = 1$, and $m_F g = 53.01N$. The data fitting results are shown in Figure 19.

Another method is to identify the parameters according to Equation (60), i.e. identifying the parameters using the normal force–sinkage data of each experiment under different loads. The data fitting results for the experiments under different vertical loads and the average values are listed in Table 10. The estimated parameters are as follows: $k_{FN} = 1.191 \times 10^4\,\mathrm{N}$, $n_{FN} = 1$, and $m_F g = 51.27\,\mathrm{N}$. The parameters identified by two different approaches of Equations (60) and (61) are approximate.

Figure 20 shows the original experimental data and the data fitting results of the deformable foot versus the hard terrain of Group 2, in which the foot is loaded with impact. The measured normal force and the foot deformation rise to the highest value and then vibrate with a damping before it reaches a steady value. The data in Figure 20(c) are used to identify the damping term parameters with Equation (60). The foot's velocity in the normal direction is obtained by differentiating z(t). The identified results are as follows: $b = 398.21\mathrm{Nm}^{1.01}\mathrm{s}^{-0.76}$, $p = 0.25$, and $q = 0.76$. Figure 20(d) shows the simulation results of z versus t using the identified parameters. The relative errors of the predicted results using the identified parameters versus the experimental results are shown in Figure 20(e), in which the time axes for different results are made aligned. The maximum relative error is approximately 10%. It is verified that the identified parameters have a reasonable fidelity in predicting the contact mechanics of the experimental deformable foot.

The experimental results of Group G_{10} are used for identifying the tangential force parameters. Three kinds of hard terrain are used: brick, marble, and steel. Tests T16, T18, and T20 use a horizontal velocity of $-20\,\mathrm{mm/s}$, whereas tests T15, T17, and T19 use a horizontal velocity of 20 mm/s. The horizontal deformation of the foot is caused

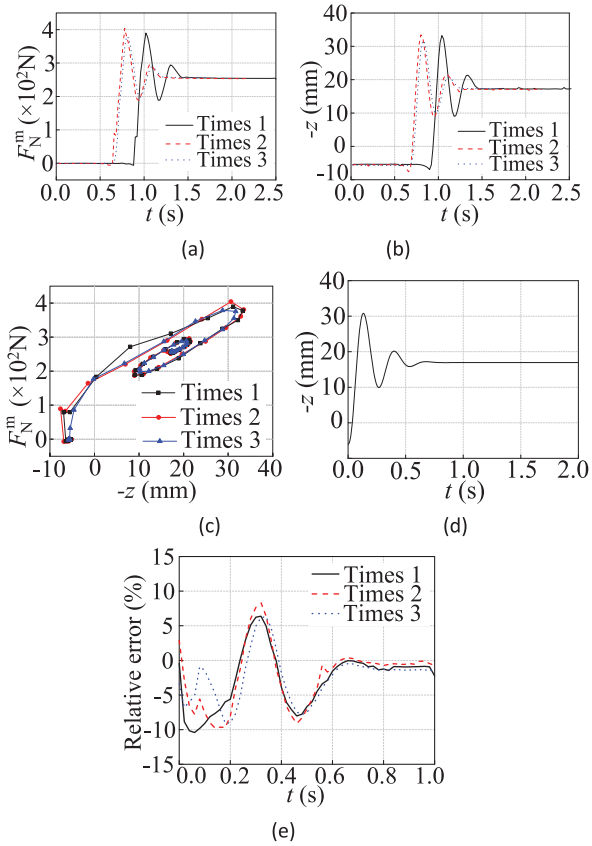

Fig. 20. Original experimental data and predicted results of deformable foot versus hard terrain (Group 2, loading with impact): (a) F_N^m versus t; (b) z versus t; (c) F_N^m versus z; (d) z versus t (predicted); (e) relative error of predicted results versus experimental results.

by the rubber pad. According to Equations (5) and (64), the normal force that acts on the foot by the terrain is as follows:

$$F_{TN} = F_N + m_F g = F_N^m. \tag{67}$$

The original experimental results and data fitting results of the tangential force are shown in Figure 21. Further, the identified parameters are tabulated in Table 11. It is verified that both Equation (37) and Equation (44) have approximate precision in predicting the tangential force as functions of the horizontal deformation and identifying the unknown parameters. The parameters μ and K are influenced by the properties of both the foot and the terrain. The foot on the brick has maximum frictional coefficient μ and deformation modulus K.

5.3. Hard foot versus deformable terrain

Figure 22 shows the original quasi-static loading experimental data of experiments for the hard foot versus the deformable terrain. Comparing with the experimental data obtained from the deformable foot on the hard terrain, there are several distinctions: (1) the normal contact force F_{TN}

Table 8. Experimental setup.

Description	Group No.	Test No.	W (N)	Foot	Terrain	Initial height
Quasi-static loading	G1	T1–T5	100, 200, 250, 300, 350	Deformable	Marble	8 mm
Loading with impact	G2	T6	250	Deformable	Marble	5 mm
Quasi-static loading	G3	T7–T11	40, 120, 200, 250, 300	Hard	Soft sand	10 mm
Loading with impact	G4	T12	250	Hard	Soft sand	5 mm
Quasi-static loading	G5	T13	250	Deformable	Soft sand	8 mm
Loading with impact	G6	T14	250	Deformable	Soft sand	5 mm
		T15–T16	120	Deformable	Brick	
	G7	T17–T18	140	Deformable	Marble	
Tangential force experiment						–
		T19–T20	140	Deformable	Steel	
	G8	T21–T22	50	Hard	Soft sand	

Table 9. Steady values of measured normal force and foot sinkage for Group 1.

	Parameter	Times 1	Times 2	Times 3	Times 4	Times 5	Average values	Standard deviation
Test 1	F_{Nm} (N)	110.81	111.13	111.05	111.53	112.60	**111.42**	0.632
	$-z$ (mm)	4.79	4.81	4.88	4.89	4.96	**4.86**	0.062
Test 2	F_{Nm} (N)	178.70	179.21	178.63	178.54	179.04	**178.82**	0.257
	$-z$ (mm)	10.57	10.56	10.55	10.53	10.56	**10.55**	0.016
Test 3	F_{Nm} (N)	251.97	252.29	251.64	251.73	252.43	**252.01**	0.307
	$-z$ (mm)	16.61	16.61	16.58	16.59	16.59	**16.60**	0.013
Test 4	F_{Nm} (N)	298.59	298.13	297.74	298.21	297.81	**298.09**	0.306
	$-z$ (mm)	20.80	20.80	20.76	20.79	20.81	**20.79**	0.018
Test 5	F_{Nm} (N)	338.85	339.31	338.54	339.48	339.00	**339.04**	0.333
	$-z$ (mm)	23.81	23.84	23.52	23.86	23.75	**23.75**	0.122

Table 10. Identified parameters and average values using the normal force-sinkage data of each experiment.

Parameter	Test 1	Test 2	Test 3	Test 4	Test 5	Average value
$k_{\mathrm{FN}}(kNm^{-1})$	12.14	11.83	11.79	11.87	11.96	**11.92**
$m_{\mathrm{F}}g(\mathrm{N})$	50.51	52.17	55.47	48.88	49.33	**51.27**

generated by the soil is equal to the measured normal force $F_{\mathrm{N}}^{\mathrm{m}}$ according to Equation (66), while the force F_{FN} generated by the foot is equal to $F_{\mathrm{N}}^{\mathrm{m}} - m_{\mathrm{F}}g$; (2) the force F_{TN} increases gradually from zero to the maximum value, without an abrupt increment from zero to $m_{\mathrm{F}}g$; (3) the exponent of rigidity term is nonlinear, as n_{TN} is determined by the soil and the foot, while the exponent of n_{FN} is 1 as the spring on the foot is linear; and (4) the normal force turns to be zero immediately when the foot begins to leave the deformable soil, which is due to the plastic deformation of the soil, but the spring has no hysteresis.

The parameters k_{TN} and n_{TN} of the model are identified using Equation (59), and the results are shown in Table 12 for different vertical loads. The average values of the different experiments are as follows: $k_{\mathrm{TN}} = 5.06 \times 10^3 \mathrm{Nm}^{-1.132}$, and $n_{\mathrm{TN}} = 1.132$. The sinkage exponent of the soil is as follows: $n = n_{\mathrm{TN}} - 0.5 = 0.632$. Although the value of k_{TN} for test 4 is much larger than that for test 1, the value of n_{TN} for test 4 is obviously smaller than that for test 1 as compensation. Note that the curves of F_{N} versus z in Figure 22(c) almost match together, which implies that the values of k_{TN} and n_{TN} may be influenced obviously by the small change in the original data, and different groups of k_{TN} and n_{TN} may obtain a similar predicted force. Figure 22(d) shows the predicted normal force with the average identified parameters, and the fidelity of the model is validated.

Figure 23 shows the original experimental data and the data fitting results of the hard foot versus the deformable terrain of Group 4, in which the foot is loaded with impact. The measured normal force and the foot deformation rise to the highest values; after that, the wheel sinkage remains constant, but the normal force abruptly turns to the value that balances with the vertical load. Equation (56) is obtained from this observation. When the velocity of the foot decreases to zero and the foot sinkage reaches the maximum absolute value, the normal force turns to $W + m_{\mathrm{F}}\mathrm{g}$ immediately to make the acceleration of the foot zero so that the foot will not move in the normal direction. The reason for this phenomenon is that the deformation of the soil is plastic and the deformable sand flows without any rebounding. The identified parameters are $b_{\mathrm{N}} = 205.07\,\mathrm{Nm}^{0.171}\mathrm{s}^{-0.075}, p_{\mathrm{N}} = 0.096, q_{\mathrm{N}} = 0.075,$

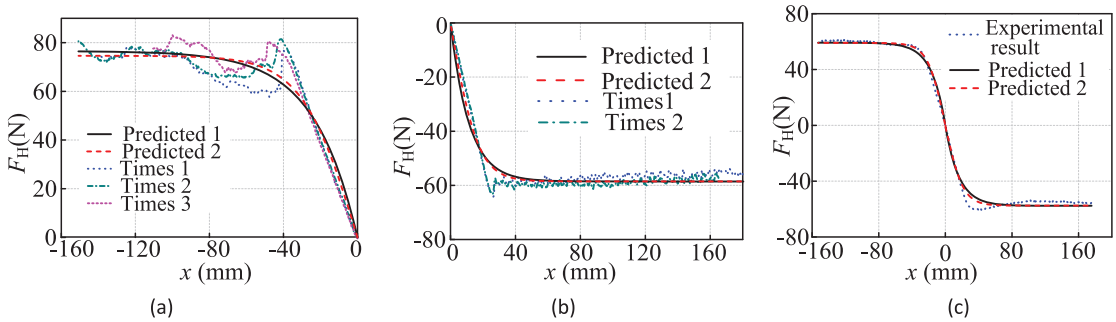

Fig. 21. Original experimental results and data fitting results of tangential force for deformable foot on hard terrain (Group G7): (a) tangential force on brick (Test T16); (b) tangential force on marble (Test T17); (c) tangential force on steel (Tests T19 and T20).

Table 11. Identified parameters of tangential force model for deformable foot on hard terrain (Group G10).

Parameters		Brick	Marble	Steel
	$F_{TN}(N)$	120.70	143.78	124.53
Method 1: Equation (62)	μ	0.634	0.407	0.469
	K (mm)	23.320	11.388	16.070
Method 2: Equation (63)	μ	0.618	0.406	0.468
	K (mm)	20.023	11.280	14.009

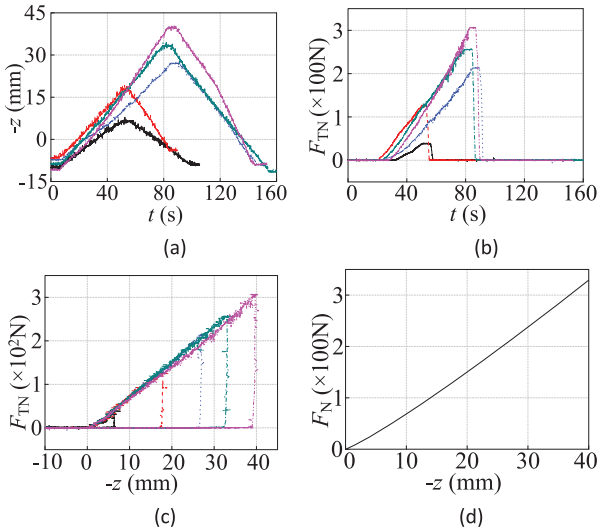

Fig. 22. Original quasi-static loading experimental data and data fitting results of hard foot versus deformable terrain (Group G3): (a) z versus t; (b) F_N versus t; (c) F_N versus z; (d) F_N versus z (predicted).

which are used to obtain the results shown in Figure 23(d). The parameters are identified using the experimental data directly, so that the estimation error of F_N as a function of time t shown in Figure 23(d) is small and the force characteristics could be reproduced with high precision. However, one should note that the entrance angle of the foot is approximately $\pi/2$, which violates the assumption of Equation (26). As a result, the simplification error of Equation (29) is large and the error cannot be neglected. If Equation (29) is used to estimate the soil property parameters according to the identified results, or to predict the interaction mechanics using the known soil parameters, the error caused by a large entrance angle should be considered for compensation.

The overshoot and abrupt decrement of the normal force is distinguished from the spring–damping system (Figure 20 is an example) in principle. The phenomenon is due to the plasticity of the soil. From the viewpoint of dynamics and kinematics, there should be an overshoot of the normal force in order to cause a deceleration to the foot. From the viewpoint of energy conservation, when the normal velocity of the foot is zero, the kinetic energy turns to zero and it is absorbed by the soil. As the plastic deformation energy is non-reversible, there is no energy to cause a normal force that is larger than the vertical load in order to generate an upward motion to the foot. So that the normal force equals to the vertical load immediately and the foot becomes steady without rebounding motion. The process is like a ball that drops on the plasticine. The energy is primarily consumed by the plastic deformation, rather than the damping related to the velocity.

Figure 24 shows the original experimental results and the data fitting results of the tangential force for a hard foot moving on the deformable terrain (Group G8). Five times of the repeated tangential force experiments, respectively, for test T21 and T22 are drawn in Figure 24(a) and (b). The foot sinkage increases from the initial value to about 70 mm, and the absolute value of the tangential forces increases from 0 to 55 N. The average vertical load ranges from 65 to 70N. The average value of all the vertical loads of different experiments is 67.11 N, and the identified parameters using Equation (63) are as follows: $c = 460$ Pa (given according to Ding et al., 2013a), $\tan\varphi = 0.852(\varphi = 40.43^\circ)$, and $K = 155.13$ mm. The predicted internal cohesion angle of the soil is close to the value (38.1°) measured with the standard shearing experiment.

Table 12. Identified parameters and average values using the force-sinkage data of each experiment (Group G3).

Parameters	Test 1	Test 2	Test 3	Test 4	Test 5	Average value
$k_{TN}(\mathrm{kNm}_{TN}^{-n})$	3.72	5.45	4.78	6.15	5.18	5.06
n_{TN}	1.232	1.109	1.151	1.068	1.099	1.132

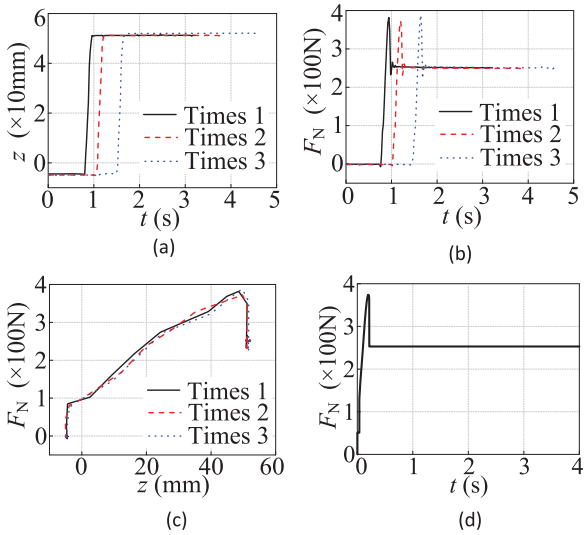

Fig. 23. Original experimental data and data fitting results of hard foot versus deformable terrain (Group G_4, loading with impact): (a) z versus t; (b) F_N versus t; (c) F_N versus z; (d) F_N versus t (predicted).

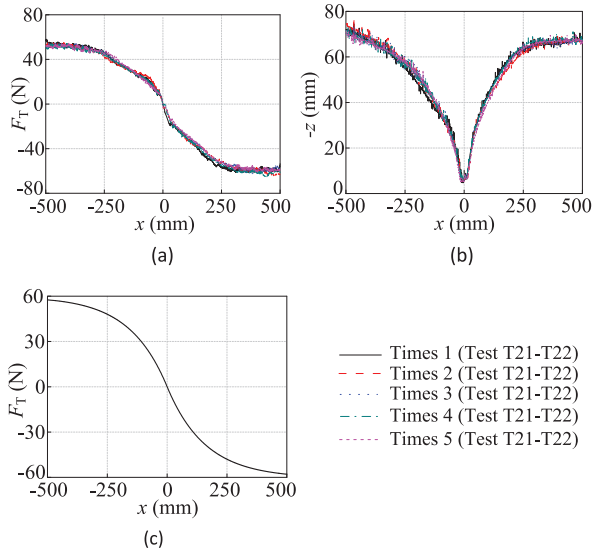

Fig. 24. Original results and data fitting results of tangential force (hard foot on deformable terrain, Group G_8): (a) F_T versus x; (b) z versus x; (c) F_T versus x.

The predicted results of the tangential force using the identified parameters and the average vertical load are shown in Figure 24(c), which are close to the experimental results.

We also noticed that the value of parameter K is much larger than those provided in the literature, such as Wong (2009). In Ding et al. (2013b), the values of K for several different kinds of soft soils are smaller than 25.4mm, and the identified K for the experimental lunar soil stimulant ranges from 13.3 to 17.2 mm. The reason of obtaining a large K is partially due to the bulldozing effect of soil. In Figure 24(b), the foot sinkage increases from several millimeters to approximately 70 mm. With the increase of foot sinkage, the bulldozing effect becomes increasingly significant, which leads to a gradual increase in the tangential force. However, the friction model does not take into account the bulldozing force explicitly. As a result, the precision of identified parameters gets lower to compensate for the model error, among which K is primarily influenced. If the tangential force model is used to predict the foot–soil interaction mechanics using the soil parameters measured by the standard shearing experiment (Wong, 2009) rather than those identified from foot–soil interaction experiments, the bulldozing force should be considered to improve the model precision. Or the horizontal displacement should be confined within a limited range in order to restrict the foot sinkage and ensure the model precision.

5.4. Deformable foot versus deformable terrain

Quasi-static loading experiments were also carried out for the deformable foot with a spring to come into contact with the deformable sand, the results of which are shown in Figures 25 and 26. The equations of the lines that agree with the original results of FN versus z are

$$\begin{cases} \mathrm{L1}: F_{TN} = 1.227 \times 10^4 z - 14.9\ (\mathrm{N}) \\ \mathrm{L2}: F_{TN} = 5.530 \times 10^3 z + 38.9\ (\mathrm{N}) \\ \mathrm{L3}: F_{TN} = 1.172 \times 10^4 (z - 0.0225) + 51.0\ (\mathrm{N}) \end{cases}. \tag{68}$$

In the beginning, the normal force F_{TN} is smaller than m_{FG} and the spring has no deformation, so the rigidity is a combination of the rubber pad and the terrain. When the spring begins to deform, the combined rigidity becomes much smaller. Immediately when the unloading process begins, the soil has no rebounding and the combined rigidity is actually that of the spring.

Loading with impact experiments were also be done for the deformable foot on the deformable terrain, as shown in Figure 27. The vibrations of z and F_N are much smaller than the deformable foot on the hard terrain but larger than the hard foot on the deformable terrain. Actually, the soil has no rebounding due to the plastic deformation, but the spring vibrates.

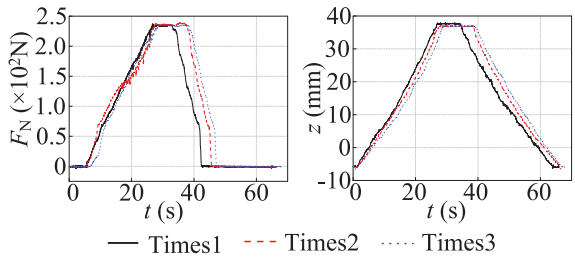

Fig. 25. Original quasi-static loading experimental data of deformable foot versus deformable terrain (Group G5).

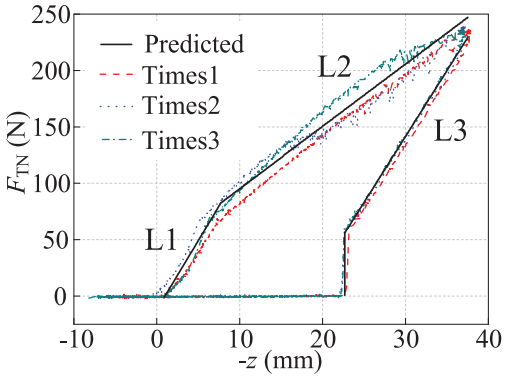

Fig. 26. Comparison of original and data fitting results for F_N versus z (Group G5).

It is not easy to analyze the deformable foot and the deformable terrain as a whole. They can be considered as a 2-DOF system, and both F_{TN} and F_{NT} have their own functions. The disadvantage of this approach is that the two groups of parameters should be measured; for instance, one should know the exact deformation of the terrain and the spring, respectively, rather than the summation of the deformation.

6. Conclusions and future work

In this paper we have investigated the modeling, parameter identification, and experimental validation of foot–soil interaction mechanics for legged robots. Several conclusions are drawn.

(1) The knowledge of terramechanics (including the Bekker model and Wong–Reece model) is adopted to deduce the normal force model of robotic feet on deformable terrains. The relationships of the normal force as the function of the terrain property parameters and the feet parameters are revealed. If a foot is flat, the normal force exponent n_{TN} is equal to the soil sinkage exponent n, whereas n_{TN} are $n+1/2$ and $n+1$ for a cylindrical foot and a spherical foot, respectively.

(2) A novel model of tangential forces as a function of displacement is proposed on the basis of the in-depth understanding of the terrain properties. It has the form of the Hunt–Crossley model, but the coefficients are the functions of the normal force, which is compatible with the Coulomb friction model.

(3) The unknown parameters of the models can be identified according to the results of both quasi-static loading experiments and loading with impact experiments for the normal force model, and the parameters of the tangential force model can be directly identified using the results of the tangential force experiment.

(4) Experiments of several groups have been carried out, including the quasi-static loading and loading with impact for the hard foot versus the deformable terrain, the deformable foot versus the hard terrain, as well as the deformable foot versus the deformable terrain. Tangential force experiments have also been performed. The experimental results are analyzed and used to validate the models and parameter identification approaches.

In the future, further research should be carried out in order to improve the adaptability and fidelity of the contact mechanics for the real legged robots. For instance, the two-dimensional contact mechanics with velocities in both the vertical and the tangential directions; experiments considering more foot parameters and motion state variables; the phenomena of the deformable foot versus the deformable terrain. Also, the foot–terrain interaction models will be applied to the development and analysis of legged robots.

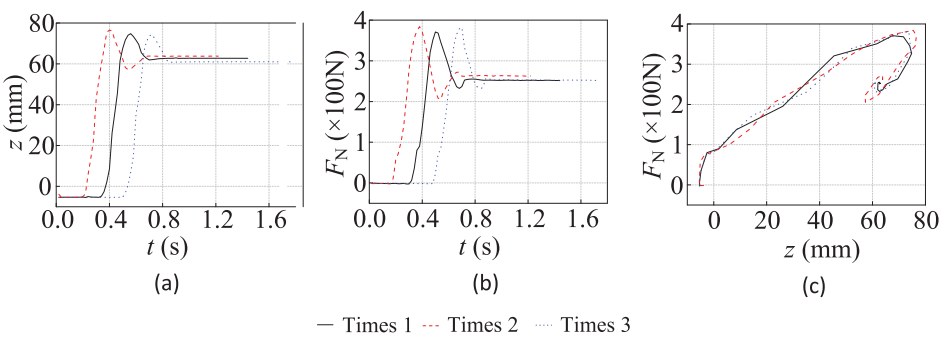

Fig. 27. Original experimental data of hard foot versus deformable terrain (Group G6, loading with impact): (a) z versus t; (b) F_N versus t; (c) F_N versus z.

Acknowledgments

The authors would like to acknowledge Professor Mantian Li and PhD candidate Zhenyu Jiang of Harbin Institute of Technology, who provided the experimental robot leg and gave some valuable advice in preparing the experiments.

Funding

This study was supported in part by the National Natural Science Foundation of China (grant number 613700 33/61005080/51275106), National Basic Research Program of China (grant number 2013CB035502), "863" Program of China (grant number 2011AA0403837002), Foundation of Chinese State Key Laboratory of Robotics and Systems (grant number SKLRS201004B), and the "111 Project" (grant number B07018).

References

Ackerman E (2012) *DARPA selects Boston Dynamics' humanoid for robotics challenge*. http://spectrum.ieee.org/automaton/robotics/humanoids/darpa-selects-boston-dynamics-humanoid-for-robotics-challenge (accessed 1 September 2012).

Bekker G (1969) *Introduction to terrain–vehicle systems*. Ann Arbor, MI: University of Michigan Press.

Biagiotti L, Melchiorri C, Tiezzi P and Vassura G (2005) Modelling and identification of soft pads for robotic hands. In *Proceedings of IEEE/RSJ International Conference on Intelligent Robots and Systems*, Edmonton, Alberta, Canada, pp. 2786–2791.

BostonDynamics (2012a) *LS3—Legged Squad Support Systems*. http://www. bostondynamics. com/robot_ls3.html (accessed 1 September 2012).

BostonDynamics (2012b) LittleDog—The Legged Locomotion Learning Robot. http://www.boston dynamics. com/robot_littledog.html (accessed 1 September 2012).

Carbone G and Ceccarelli M (2005) Legged robotic systems. In: *Cutting Edge Robotics ARS Scientific Book*, Wien, pp. 553–576.

Ding L, Deng ZQ, Gao HB, et al. (2013a) Experimental study and analysis of the wheels' steering mechanics for planetary exploration WMRs moving on deformable terrain. *The International Journal of Robotics Research*, 32 (6): 712–743.

Ding L, Deng ZQ, Gao HB, Nagatani K and Yoshida K (2011a) Planetary rovers' wheel–soil interaction mechanics: new challenges and applications for wheeled mobile robots. *Journal of Intelligent Service Robotics* 4(1): 17–38.

Ding L, Deng ZQ, Gao HB, Tao JG, Iagnemma K and Liu GJ (2013b) Contact mechanics model of driving wheels for planetary WMRs moving on deformable soil considering multiple effects. *Journal of Field Robotics*, submitted.

Ding L, Gao HB, Deng ZQ, Nagatani K and Yoshida K (2011b) Experimental study and analysis on driving wheels' performance for planetary exploration rovers moving in deformable soil . *Journal of Terramechanics* 48(1): 27–45.

Ding L, Nagatani K, Sato K, et al. (2010) Terramechanics-based high-fidelity dynamics simulation for wheeled mobile robot on deformable rough terrain. In *Proceedings of 2010 IEEE International Conference on Robotics and Automation*, Anchorage, AK, pp. 4922-4927.

Ding L, Yoshida K, Nagatani K, Gao HB and Deng ZQ (2009) Parameter identification for planetary soil based on decoupled analytical wheel–soil interaction terramechanics model. In *Proceedings of 2009 IEEE/RSJ International Conference on Intelligent Robots and Systems*, St. Louis, MO, pp. 4122–4127.

Diolaiti N, Melchiorri C and Stramigioli S (2005) Contact impedance estimation for robotic systems. *IEEE Transactions on Robotics* 21(5): 925–935.

Fujimoto Y and Kawamura A (1998) Simulation of an autonomous biped walking robot including environmental force interaction. *IEEE Robotics and Automation Magazine* 5(2): 33–42.

Gilardi G and Sharf I (2002) Literature survey of contact dynamics modeling. *Mechanism and Machine Theory* 37(10): 1213–1239.

Hardarson F (1997) *Locomotion for difficult terrain*. Technical Report, Mechatronics Division, Department of Machine Design, Royal Institute of Technology, Stockholm, Sweden.

Hunt KH and Crossley FRE (1975) Coefficient of restitution interpreted as damping in vibroimpact. *Journal of Applied Mechanics*, *Series E* 42(2): 440–445.

Hurmuzlu Y, Genot F and Brogaliato B (2004) Modelling, stability and control of biped robots—a general framework. *Automatica* 40(10): 1647–1664.

Irawan A and Nonami K (2011) Optimal impedance control based on body inertia for a hydraulically driven hexapod robot walking on uneven and extremely soft terrain. *Journal of Field Robotics*, 28(5): 690–713.

Janosi Z and Hanamoto B (1961) Analytical determination of drawbar Pull as a function of slip for tracked vehicle in deformable soils. In *Proceedings of the 1st International Conference of ISTVE*S, Torino, Italy, pp. 707–726.

Komizunai S, Konno S, Abiko A and Uchiyama M (2011) Slip characteristics identification for biped walking of a humanoid robot on sand. In *Proceedings of Eighth International Conference on Flow Dynamics*, 9–11 November 2011, pp. 622–623.

Kraus PR and Kumar V (1997) Compliant contact models for rigid body collisions. In *Proceedings of the IEEE International Conference on Robotics and Automation*, Albuquerque, NM, pp. 1382–1387.

Lankarani HM and Nikravesh E (1990) A contact force model with hysteresis damping for impact analysis of multibody systems. *Journal of Mechanical Design* 112(3): 369–376.

Li C, Zhang T and Goldman DI (2013) A terradynamics of legged locomotion on granular media. *Science* 339(6126): 1408–1412.

Maclou JM (2012) Unusual off-land locomotion. http://www.unusuallocomotion.com/pages/more-documentation/walking-hopping-sphereical-and-wsl-robots-and-vehicles.html (accessed 25 December 2012).

Mahapatra A and Roy SS (2009) Computer aided dynamic simulation of six-legged robot. *International Journal of Recent Trends in Engineering* 2(2): 146–151.

Misra M, Reed KB, Schafer BW, Ramesh KT and Okamura AM (2010) Mechanics of flexible needles robotically steered through soft tissue. *The International Journal of Robotics Research* 29(13): 1640–1660.

Nanayakkara T, Byl K, Liu H, Song X and Villabona T (2012) Dominant sources of variability in passive walking. In *Proceedings of the IEEE International Conference on Robotics and Automation*, River Centre, Saint Paul, MN, pp. 1003–1010.

Nayfeh AH and Mook DT (2004) *Nonlinear oscillations*. Wiley-VCH.

Olsson H, Åström KJ, Wit CC, et al. (1998) Friction models and friction compensation. *European Journal of Control* 4(3): 176–195.

Palis F, Rusin V, Schmucker U, Schneider A and Zavgorodniy Y (2005) Walking robot with force controlled legs and articulated body. In *Proceedings of the 15th International Symposium on Measurement and Control in Robotics*, Brussels, Belgium.

Raibert M, Blankespoor K, Nelson GR and the BigDog Team (2008) Bigdog, the rough-terrain quadruped robot. In *Proceedings of the 17th World Congress, The International Federation of Automatic Control (IFAC)*, Seoul, Korea, pp. 10822–10825.

Sanchez TG (2009) *Artificial Vision in the NAO Humanoid Robot*. Master thesis of Department of Computer Science and Mathematics, Rovira i Virgili University.

Santos PG, Cobano JA, Garcia E, Estremera J and Armada MA (2007) A six-legged robot-based system for humanitarian demining missions. *Mechatronics* 17: 417–430.

Shapiro A, Rimon E and Burdick JW (2004) On the mechanics of natural compliance in frictional contacts and its effect on grasp stiffness and stability. In *Proceedings of 2004 IEEE International Conference on Robotics and Automation*, New Orleans, LA, pp. 1264–1269.

Sharf I, Bruyninckx H, Swevers J and Schutter D (2009) Identification of contact dynamics parameters for stiff robotic payloads. *IEEE Transactions on Robotics* 25(2): 240–252.

Shibly H, Iagnemma K and Dubowsky S (2005) An equivalent soil mechanics formulation for rigid wheels in deformable terrain, with application to planetary exploration rovers. *Journal of Terramechanics* 42(1): 1–13.

Shigeo H, Yasushi F and Kan Y (2009) Quadruped walking robots at Tokyo Institute of Technology. *IEEE Robotics and Automation Magazine* 16(2): 104–114.

Silva MF, Barbosa RS and Machado JAT (2009) Development of a genetic algorithm for the optimization of hexapod robot parameters. In *Proceedings of the International Conference on Applied Simulation and Modelling*, Palma de Mallorca, Spain, pp. 77–82.

Silva MF, Machado JAT and Lopes AM (2005) Modelling and simulation of artificial locomotion systems. *Robotica* 23(5): 595–606.

Song JH (2012) *Dynamics simulation for hexapod robot based on modeling of foot–terrain interaction*. Master dissertation of Harbin Institute of Technology, Harbin, China.

Song P, Kraus P, Kumar V and Dupont P (2000) Analysis of rigid body dynamic models for simulation of systems with frictional contacts. *Journal of Applied Mechanics* 68: 118–128.

Spagna JC, Goldman DI, Lin PC, Koditschek DE and Full RJ (2007) Distributed mechanical feedback in arthropods and robots simplifies control of rapid running on challenging terrain. *Bioinspiration and Biomimetics* 2: 9–18.

Spenko MJ, Haynes GC, Saunders JA, et al. (2008) Biologically inspired climbing with a hexapedal robot. *Journal of Field Robotics* 25(4–5): 223–242.

Stewart DE (2000) Rigid-body dynamics with friction and impact. *SIAM Review* 42(1): 3–39.

Stronge WJ (1990) Rigid body collisions with Friction. *Proceedings of the Royal Society London A* 431(1881): 169–181.

Stronge WJ (1991) Unraveling paradoxical theories for rigid body collisions. *Journal of Applied Mechanics* 58: 1049–1055.

Sun Y and Ma SG (2011) Decoupled kinematic control of terrestrial locomotion for an ePaddle-based reconfigurable amphibious robot. In *Proceedings of 2011 IEEE International Conference on Robotics and Automation*, Shanghai, China, pp. 1223–1228.

Trinkle J, Pang JS, Sudarsky S and Lo G (1997) On dynamic multi-rigid-body contact problems with Coulomb friction. *Zeitschrift für Angewandte Mathematik und Mechanik* 77: 267–279.

Wahde M and Pettersson J (2002) A brief review of bipedal robotics research. In *Proceedings of the 8th UK Mechatronics Forum*, University of Twente, the Netherlands, pp. 480–488.

Wang Y and Mason MT (1992) Two-dimensional rigid-body collisions with friction. *Journal of Applied Mechanics* 59(3): 635–642.

Watanabe R, Aoyama C, Matsunaga S, Higaki N and Fujimura K (2002) The intelligent ASIMO: system overview and integration. In *Proceedings of IEEE/RSJ International Conference on Intelligent Robots and Systems*, Lausanne, Switzerland, 2002, pp. 2478–2483.

Wheeler D, Chavez-Clemente D and SunSpiral V (2010) FootSpring: a compliance model for the ATHLETE family of robots. In *Proceedings of 10th International Symposium on Artificial Intelligence*, Sapporo, Hokkaido, Japan. http://ti.arc.nasa.gov/publications/1788/download/.

Wilcox BH, Litwin T, Biesiadecki J, et al. (2007). Athlete: a cargo handling and manipulation robot for the moon. *Journal of Field Robotics* 24(5): 421–434.

Wong JY (2008) *Theory of ground vehicles* (4th edn). Hoboken, NJ: John Wiley and Sons.

Wong JY (2009) *Terramechanics and off-road engineering* (2nd edn). Amsterdam: Elsevier.

Wong JY and Reece AR (1967) Prediction of rigid wheel performance based on analysis of soil-wheel stresses, part I–performance of driven rigid wheels. *Journal of Terramechanics* 4(1): 81–98.